<u>Title page</u>

Type of the study:
Research Paper

Titel:
Path Selection and Network Equilibrium Under Non-Extreme Flood Disturbances

Author names and affiliations:
Yifan Wang [a, *]
Ryuichi Tani [a]
Kenetsu Uchida [a]

[a] Mr. Yifan Wang (corresponding author)
Graduate School of Engineering, Hokkaido University
North 13 West 8 Kita-ku, Sapporo 060-8628, Japan
yifan.wang.l6@elms.hokudai.ac.jp
ORCID: https://orcid.org/0009-0008-6891-8447

[a] Dr. Ryuichi Tani
Graduate School of Engineering, Hokkaido University
North 13 West 8 Kita-ku, Sapporo 060-8628, Japan
r-tani@eng.hokudai.ac.jp
ORCID: https://orcid.org/0000-0002-1035-2128

[a] Prof. Kenetsu Uchida
Graduate School of Engineering, Hokkaido University
North 13 West 8 Kita-ku, Sapporo 060-8628, Japan
uchida@eng.hokudai.ac.jp
ORCID: https://orcid.org/0000-0001-9316-9240

Corresponding author:
Mr. Yifan Wang [a, *]
Graduate School of Engineering, Hokkaido University
North 13 West 8 Kita-ku, Sapporo 060-8628, Japan
E-mail: yifan.wang.l6@elms.hokudai.ac.jp
Tel: +86-13253566117

Path Selection and Network Equilibrium Under Non-Extreme Flood Disturbances

Yifan Wang [a, *] (corresponding author), Ryuichi Tani [a], Kenetsu Uchida [a]

[a] *Graduate School of Engineering, Hokkaido University, Sapporo, Japan*

Abstract

Non-extreme flood disasters caused by urban fluvial flooding can disrupt and impact the operation of urban road traffic systems. This is particularly evident in the influence on the path selection behavior of network users and the resulting changes in the equilibrium state of the road network. Consequently, the network cannot maintain its original performance, leading to disturbances and interruptions. Therefore, this study proposes a novel stochastic traffic assignment model to simulate and analyze such scenarios. The model proposed in this study introduces a path cost expression that incorporates two stochastic terms, effectively capturing the perceived objective costs for different types of users under non-extreme flooding: flood risk and travel time, as well as the subjective cost factors of the users. Additionally, this study introduces a new criterion to classify paths into acceptable and unacceptable categories. Users will abandon unacceptable paths deemed too dangerous and will choose paths only from their set of acceptable paths until the road network reaches an equilibrium state. The corresponding set of acceptable paths will dynamically change based on the risk sensitivity of different types of users and the prevailing flood conditions. The model developed in this study can effectively analyze the impact of non-extreme floods on the path selection behavior of users with different risk sensitivities and simulates the evolution of the road network's equilibrium state as users instinctively avoid risks. This research provides valuable insights for stakeholders in the operation, management, maintenance, and restoration of road networks under non-extreme flood conditions.

Keywords: Risk Sensitivity; Non-extreme Flood; User Path Selection, Path Choice Set.

1. Introduction

1.1 Background

Urban flood disasters can be categorized into pluvial flooding, fluvial flooding, and coastal flooding (Agonafir et al., 2023). Given the increasing frequency of extreme weather events worldwide, urban pluvial flood disasters triggered by extreme rainfall are becoming more severe (Ren et al., 2024, Ai et al., 2024, Patwary et al., 2024). Urban pluvial flooding directly impacts the normal operation of road network infrastructure, affecting driver mobility and potentially leading to disruptions in the road network, resulting in significant economic losses and even threatening driver' lives (Koetse and Rietveld, 2009, Patil et al., 2024). Due to the complex nature of extreme rainfall events, urban pluvial flood disasters exhibit diverse intensities, which in turn affect the path selection of users within the road network and influence the assignment of traffic flow and equilibrium state of the network, and further impacting the performance of the road network in terms of resilience and accessibility. Therefore, analyzing the assignment of traffic flow within the road network under the influence of urban pluvial flood disasters plays a crucial role in facilitating the management, maintenance, operation, and repair of the road network in the face of flood impacts, and particularly facilitates further research on the resilience of transportation networks under the impact of non-extreme floods.

1.2 Literature Review

(1) Flood disasters in transportation networks

Urban pluvial flooding refers to floods triggered by a sudden and intense rainfall, leading to a rapid increase in surface runoff due to the high impervious surface coverage and inadequate drainage system capacity in urban areas (Gradeci et al., 2019). The extent of damage caused by rainfall floods is closely related to rainfall intensity and urban drainage capacity (Wang et al., 2016). Extreme flood disasters occurring in cities often result in significant damage to urban infrastructure systems, especially the road network system, affecting accessibility and causing substantial property losses or even endangering lives (Acosta-Coll et al., 2018). In contrast to extreme floods, non-extreme flood disasters occur when short-term rainfall is not

*Corresponding author.
E-mail address: yifan.wang.l6@elms.hokudai.ac.jp

extremely intense but still exceeds the capacity limits of the urban drainage system (Li et al., 2019). While non-extreme floods may not directly paralyze the entire transportation network system, leading users to abandon their travel plans entirely (Van Ootegem et al., 2015), they do impact users' path selection behavior, which in turn alters the traffic flow assignment across the network (He et al., 2023). This impacts the overall efficiency of the network and results in diminished performance. Compared to extreme floods, the effects of non-extreme floods on the network tend to be more widespread and prolonged, often leading to significant indirect financial losses. Hence, investigating traffic assignment issues under the influence of non-extreme floods is equally imperative, which will provide positive impetus for stakeholders in the transportation system to manage and maintain road networks effectively. Although many current studies assume flood disasters as perturbing factors in the analysis of transportation networks—such as accessibility (Zhou et al., 2022, He et al., 2021), vulnerability (Sullivan et al., 2023, Ye and Kim, 2019), and resilience (Fang et al., 2023, Ma et al., 2023, Chen and Rose, 2018) under flood disturbances—most of these studies consider the extreme flood scenarios. There is limited research on the impacts of non-extreme floods. Therefore, incorporating non-extreme flood scenarios into the analysis could advance research in this area and provide valuable insights for real-world network management and maintenance during non-extreme flood events.

On the other hand, when a flood occurs in the road network, users with different levels of risk sensitivity exhibit distinct path selection behaviors. Even for the same path submerged by non-extreme floods, less risk-sensitive users might still opt for it, whereas those more sensitive to risks would avoid it. This implies that, on the same network and between the same origin-destination (O-D) pairs, the path sets selected by users with different levels of risk sensitivity differ when a flood transpires. However, scant scholarly attention has been paid to this phenomenon. Therefore, exploring the dynamic changes in path sets for traffic assignment in relation to changes in user risk sensitivity and flood scenarios holds significant relevance.

(2) Reliability-based network equilibrium

Travel time reliability is one of the key factors users consider when selecting paths (Jackson and Jucker, 1982, Abdel-Aty et al., 1995), especially when the network is impacted by disasters such as floods, heavy rainfall, or earthquakes. In such scenarios, users instinctively seek to avoid risk, and the reliability of travel time often outweighs purely minimizing travel time costs in their decision-making (Liu et al., 2004). When a non-extreme flood occurs, although it may not force users to abandon their travel plans entirely, the uncertainty and safety risks associated with the flood can significantly influence path selection behavior, thereby altering the original network equilibrium state. Compared to traditional traffic assignment methods based on the user equilibrium principle, models that account for travel time reliability are better suited to capturing the impact of uncertainty on users' path selections and analyzing changes in network equilibrium (Carrion and Levinson, 2013, Carrion and Levinson, 2012). Consequently, numerous reliability-based network equilibrium models have been developed. Lo et al. (2006) proposed the concept of travel time budget and developed a within the budgeted time network equilibrium model. Watling (2006) proposed a reliability-based equilibrium model that utilized a path cost function incorporating stochastic travel time and late arrival penalty. Chen and Zhou (2010), Xu et al. (2014) developed the mean-excess traffic equilibrium model, in which travelers always choose the route with the least impact from unreliability, ensuring path reliability. de Palma and Picard (2005), Nikolova and Stier-Moses (2014) used a linear combination of the mean and variance of random travel times to construct a corresponding reliability-based network equilibrium model. Siu and Lo (2014) developed a model that analyzes travelers' route and departure time choices based on the need to ensure punctuality, considering the trade-off between travel time reliability and the risk of arriving late. Among the many reliability-based network equilibrium models, some scholars have considered the disturbances caused by adverse weather or natural disasters and developed corresponding network equilibrium models based on the characteristics of these disasters. For example, Sumalee et al. (2011) analyzed the uncertainty effects on both the demand and supply sides under severe weather conditions and constructed a corresponding reliability-based network equilibrium model with a focus on the mean-variance framework. Lam et al. (2008) incorporated a random term into the route cost function to capture the uncertainty caused by heavy rain and developed a corresponding reliability-based network equilibrium model.

While some scholars have constructed reliability-based equilibrium models that consider natural disasters as perturbing factors, very few studies have focused on the reliability-based network equilibrium models based on the characteristics of non-extreme floods. Therefore, this research assumes non-extreme floods as a perturbing factor for the network and conducts analysis accordingly. In reliability-based network equilibrium models, most models express the impact of uncertainty on users' perceived costs by incorporating a random term into the path cost function. When a flood disaster occurs, users face not only time costs but also flood risks, and users' subjective psychological factors also influence their path selections. However, many current reliability-based network equilibrium models rarely consider the combined effects of time costs, risk costs, and psychological factors in path selection. This study incorporates all these influencing factors into the cost function. Furthermore, these factors often exhibit uncertainty, so one single random term in the path cost function is insufficient. While current reliability-based network equilibrium models always include only one random term in the cost function, this study's path cost function employs two random terms with different distributions to better capture the uncertainties associated with various influencing factors.

(3) Bounded rationality network equilibrium

In real-world networks, users face limitations in information availability, computational capacity, and time, preventing them from making fully rational decisions when selecting paths (Simon, 1955). Consequently, bounded rationality theory assumes that users can only select the optimal or suboptimal paths within a constrained set of options. The decision-making logic proposed by bounded rationality better reflects the actual behavior of users in real-world scenarios, leading to the development of various network equilibrium models that account for bounded rationality. Di et al. (2013) discussed the impact of bounded rationality on network equilibrium states, while Fosgerau and Small (2013) analyzed congestion in traffic networks in the context of bounded rationality. Mahmassani and Liu (1999) explored the dynamic effects of bounded rationality on users' travel decisions during the process of information acquisition. Siri et al. (2022) proposed a day-to-day path selection model based on bounded rationality and validated it empirically. Bounded rationality-based network equilibrium models typically set tolerance thresholds or constraints, allowing for a certain degree of suboptimal choices, thereby avoiding the strict conditions imposed by fully rational user equilibrium and system optimal states.

In the context of non-extreme flood events, certain routes may be deemed unacceptable by users and thus avoided. The determination of these unacceptable routes is influenced by the flood conditions and users' risk sensitivity. However, in existing studies on network equilibrium under flood impact, few have simultaneously linked users' path choice sets to flood conditions and risk sensitivity. On the other hand, in studies employing Logit-type models for traffic assignment, even routes with very high costs are assigned some traffic flow, which is clearly inconsistent with real-world behavior under flood disturbances. Inspired by bounded rationality theory, this study proposes a new path selection criterion that links tolerance thresholds to flood conditions and user risk sensitivity, ensuring that unacceptable paths are excluded first. Subsequently, users will select the most reliable path from the remaining options. This dynamic adjustment of the path choice set, influenced by both risk sensitivity and flood conditions, allows for a more effective analysis of user path selection behavior under non-extreme flood impacts.

1.3 Research Contents

Based on the current research status outlined above, conducting an analysis of traffic flow assignment considering non-extreme flood scenarios and accounting for the varying risk sensitivities of different users would be highly meaningful. Therefore, this paper takes the backdrop of non-extreme flood where users do not entirely forsake travel plans, categorizes users based on the level of risk sensitivity, a link-based traffic assignment model with cost function incorporating binary stochastic terms (BST model) is designed to investigate the path selection behavior of different user types under the influence of non-extreme flood. Compared with conventional model, the cost function in the BST model comprises three components: travel time, flood risk, and path selection inertia. Path travel time is determined on a 'link-based' method, factoring in user risk sensitivity. Flood risk is determined by the length, depth, and velocity of flooding along the links. Travel time and flood risk together constitute the objective costs considered by users during path selection, while path selection inertia represents users' subjective psychological factors. Both flood risk and path selection inertia in the cost function are stochastic variables, which are incorporated to reflect the ambiguity perceived by users and the uncertainty of subjective psychological factors. And the BST model also introduces novel criteria for path selection, wherein paths are categorized into 'acceptable paths' and 'unacceptable paths' based on user risk sensitivity. Users of corresponding categories only select paths from their respective acceptable path sets, ensuring that no traffic is allocated to the unacceptable path sets. Furthermore, the BST model proposes new path equilibrium conditions, aiming to dynamically adjust the acceptable path set in response to changes in user risk sensitivity and non-extreme flood conditions, and effectively simulate the traffic assignment status of road networks under non-extreme flood conditions.

2. Path Cost Function

The notations employed in this paper are shown in Appendix A.

2.1 User Classification and Path Flow

Users within each O-D pair are categorized into different types based on their risk sensitivity, denoted as ρ_{im}, where m represents the user type. User risk sensitivity represents the degree of concern towards risks, with higher sensitivity indicating greater aversion to risks. Users with different levels of risk sensitivity will perceive different travel costs for the same paths and will make different path choices accordingly. This study assumes that the demand for O-D pair Q_i, $i \in I$, is a random variable, denoted as $Q_i \sim (q_i, \sigma_i^2)$. Employing Q_{im} represents the demand for different types of users within the same O-D pair. Q_{im} is stochastic, denoted as $Q_{im} \sim (q_{im}, \sigma_{im}^2)$, and Q_{im} is independent of each other. Then the following relationship holds:

$$Q_i = \sum_{m \in M_i} Q_{im} \quad \forall i \in I \tag{1}$$

$$Q_{im} = P_{im} \cdot Q_i \quad \forall i \in I, \forall m \in M_i \tag{2}$$

$$q_{im} = P_{im} \cdot q_i \quad \forall i \in I, \forall m \in M_i \tag{3}$$

$$\sigma_{im}^2 = var[Q_{im}] = (P_{im})^2 \cdot var[Q_i] = (P_{im})^2 \cdot \sigma_i^2 \quad \forall i \in I, \forall m \in M_i \tag{4}$$

where P_{im} represents the proportion of Q_{im} occupied in Q_i. F_{imj} denotes the stochastic traffic flow on the path $j \in J_i$ belonging to Q_{im}, denoted as $F_{imj} \sim (f_{imj}, \sigma_{imj}^2)$. And introducing P_{imj} to denote the proportion of traffic flow among different paths within Q_{im}, which is interpreted as the probability of user type 'm' selection among different paths within Q_{im}. Then the following relationship can be obtained:

$$Q_{im} = \sum_{j \in J_i} F_{imj} \quad \forall i \in I, \forall m \in M_i \tag{5}$$

$$F_{imj} = P_{imj} \cdot Q_{im} \quad \forall i \in I, \forall m \in M_i, \forall j \in J_i \tag{6}$$

$$f_{imj} = P_{imj} \cdot q_{im} \quad \forall i \in I, \forall m \in M_i, \forall j \in J_i \tag{7}$$

$$\sigma_{imj} = \sqrt{var[F_{imj}]} = \sqrt{var[P_{imj} \cdot Q_{im}]} = P_{imj} \cdot \sigma_{im} \quad \forall i \in I, \forall m \in M_i, \forall j \in J_i \tag{8}$$

$$cov[F_{imj}, F_{imk}] = cov[P_{imj} \cdot Q_{im}, P_{imk} \cdot Q_{im}] = P_{imj} \cdot P_{imk} \cdot \sigma_{im}^2 \quad \forall i \in I, \forall m \in M_i, \forall j, k \in J_i \tag{9}$$

F_{ij} represents the total stochastic traffic flow on the path $j \in J_i$, as $F_{ij} \sim (f_{ij}, \sigma_{ij}^2)$, and V_a represents the total stochastic flow on the link a, as $V_a \sim (v_a, \sigma_a^2)$. The following relationship holds:

$$f_{ij} = \sum_{m \in M_i} f_{imj} \quad \forall i \in I, \forall j \in J_i \tag{10}$$

$$var[F_{ij}] = \sigma_{ij}^2 = \sum_{m\in M_i} var[F_{imj}] = \sum_{m\in M_i} \sigma_{imj}^2 \quad \forall i \in I, \forall j \in J_i \tag{11}$$

$$cov[F_{ij}, F_{ik}] = \sum_{m\in M_i} cov[F_{imj}, F_{imk}] = \sum_{m\in M_i} P_{imj} \cdot P_{imk} \cdot \sigma_{im}^2 \quad \forall i \in I, \forall j, k \in J_i \tag{12}$$

$$V_a = \sum_{i\in I} \sum_{j\in J_i} \delta_{aj} \cdot F_{ij} \quad \forall a \in A \tag{13}$$

$$v_a = \sum_{i\in I} \sum_{j\in J_i} \delta_{aj} \cdot f_{ij} \quad \forall a \in A \tag{14}$$

$$\sigma_a^2 = \sum_{i\in I} \sum_{j\in J_i} \delta_{aj} \cdot var[F_{ij}] + \sum_{i\in I} \sum_{j\in J_i} \sum_{k\in J_i, k\neq j} \delta_{aj} \cdot \delta_{ak} \cdot cov[F_{ij}, F_{ik}] \quad \forall a \in A \tag{15}$$

$$cov[V_a, V_b] = \sum_{i\in I} \sum_{j\in J_i} \sum_{k\in J_i} \delta_{aj} \cdot \delta_{ak} \cdot cov[F_{ij}, F_{ik}] \quad \forall a, b \in A \tag{16}$$

2.2 Construction of Path Cost Function

The acquisition of link travel times is based on the BPR function, as depicted below:

$$T_a = t_a^0 \left(1 + \beta \left(\frac{V_a}{C_a}\right)^\lambda\right) \quad \forall a \in A \tag{17}$$

where t_a^0 is the free flow travel time on the link a. T_a is stochastic, then the mean $E[T_a]$ and variance $var[T_a]$ can be obtained:

$$E[T_a] = t_a^0 + \frac{t_a^0 \cdot \beta}{C_a^R} \cdot E[V_a^\lambda] \quad \forall a \in A \tag{18}$$

$$var[T_a] = \left(\frac{t_a^0 \cdot \beta}{C_a^\lambda}\right)^2 \cdot \left(E[V_a^{2\cdot\lambda}] - \left(E[V_a^\lambda]\right)^2\right) \quad \forall a \in A \tag{19}$$

(1) Perceived Path Travel Time

In the context of non-extreme flood, risk sensitivity significantly affects users' perception of travel time. Users with higher risk sensitivity tend to dislike risks more, leading them to perceive longer travel times and thus prioritize reliability in their travels. To reflect the impact of risk sensitivity on users' perception of travel time, this study adopts the approach of link-based travel time reliability measures based on the sub-additivity property, as the corresponding reliability-based travel time calculation formulas used by Xu et al. (2017). Then this study constructs the mathematical expressions that represents the relationship between risk sensitivity and perceived travel time. Let t_{ima} represent the perceived link travel time for m-type users within an O-D pair under their own risk sensitivity influence. The way t_{ima} represents the user-perceived link travel time and its specific calculation expression are as follows (the detailed derivation of the calculation expression can be found in Appendix B):

$$\Pr(T_a < t_{ima}) \geq \rho_{im} \quad \forall i \in I, \forall m \in M_i, \forall a \in A \tag{20}$$

$$t_{ima} = E[T_a] + \sqrt{\frac{\rho_{im}}{1-\rho_{im}}} \cdot \sqrt{var[T_a]} \quad \forall i \in I, \forall m \in M_i, \forall a \in A \tag{21}$$

By directly summing t_{ima}, the perceived path travel time for type m users can be obtained, denoted as t_{imj}. The specific expression is as follows:

$$t_{imj} = \sum_{a\in A} \delta_{aj} \cdot t_{ima} \quad \forall i \in I, \forall m \in M_i, \forall j \in J_i \tag{22}$$

The method represented by Equations (20), (21), and (22) for calculating the perceived path travel time of users is termed the 'link-based method'. In contrast, the more commonly used 'path-based method' involves first calculating the corresponding path travel time and then determining the user's perceived path travel time based on this, as shown below:

$$\begin{cases} E\left[T_{ij}\right] = \sum_{a\in A} \delta_{aj} \cdot E[T_a] \\ var\left[T_{ij}\right] = \sum_{a\in A}\sum_{b\in A} \delta_{aj} \cdot \delta_{bj} \cdot cov[T_a, T_b] \\ \Pr\left(T_{ij} < t_{imj}^{path-based}\right) \geq \rho_{im} \\ t_{imj}^{path-based} = E\left[T_{ij}\right] + \sqrt{\frac{\rho_{im}}{1-\rho_{im}}} \cdot \sqrt{var\left[T_{ij}\right]} \end{cases}$$

$$\forall i \in I, \forall j \in J_i, \forall m \in M_i, \forall a \in A \quad (23)$$

Whether adopting a link-based or path-based method, the key lies in the use of the calculation method proposed in Appendix B for user-perceived travel time, as indicated by '$E[\cdot] + \sqrt{\frac{\rho_{im}}{1-\rho_{im}}} \cdot \sqrt{var[\cdot]}$', for simplicity, $\rho(\cdot)$ is used to represent it. Under the impact of flood disasters, longer travel times imply a greater likelihood of users encountering danger. Therefore, perceived travel time not only carries the characteristics of time cost but also embodies a distinctive risk attribute. When considering the risk attribute of perceived travel time, the calculation method represented by $\rho(\cdot)$ serves as a risk measure. For a reasonable risk measure, sub-additivity is a necessary condition. Hence, ensuring that $\rho(\cdot)$ possesses sub-additivity to reflect the risk characteristics of perceived travel time provides additional advantages. Let X represent the travel time T_a for link a, and Y represent the travel time T_b for link b. The travel time T_{ij} for path j, composed of links a and b, is given by $X + Y$. Thus, the following relationship holds (The proof process is provided in Appendix C):

$$\rho(X+Y) \leq \rho(X) + \rho(Y) \quad (24)$$

The left side of Equation (24) can be regarded as the 'path-based method', while the right side can be regarded as the 'link-based method'. Equation (24) demonstrates that the method represented by $\rho(\cdot)$ for calculating perceived travel time satisfies the 'sub-additivity of risk measure'. Thus, the mathematical expression $\rho(\cdot)$ proposed in this study for calculating perceived travel time not only effectively quantifies the impact of risk sensitivity on users' perceptions but also helps to reflect the risk characteristics of perceived travel time under flood conditions. Additionally, the relationship expressed by Equation (24) can be interpreted as the perceived travel time along a path not exceeding the sum of perceived travel times across all links within that path. Moreover, whether using a link-based or path-based method, both approaches employ mathematical expression $\rho(\cdot)$. However, considering the computational feasibility and tractability for large-scale network applications, this study adopts the link-based method to calculate the final perceived path travel time.

(2) Perceived Path Flood Risk

Flood risk on a specific link within the road network is determined by the velocity, depth, and length of flooding on that link. Leveraging mechanical principles, Martínez-Gomariz et al. (2018), Wang et al. (2021) conducted a study on the stability of vehicles under the influence of flood depth and flow velocity, providing corresponding analytical expressions. Let 'ϑ_a'denote the degree of objective risk for a vehicle to lose stability under certain flood depths and flow velocities on the link a, which can be calculated using the following formula:

$$\vartheta_a = \min\left(1, \frac{U_{af}}{U_{ac}}\right) \quad \forall a \in A \quad (25)$$

$$U_{ac} = w_1 \cdot \left(\frac{h_{af}}{h_c}\right)^{w_2} \sqrt{2 \cdot g \cdot l_c \cdot \left[{(\rho_c \cdot h_c)}/{(\rho_f \cdot h_{af})} - R_f\right]} \quad \forall a \in A \quad (26)$$

where h_{af} and U_{af} represent the flood depth and flood velocity on link a, respectively. These two key parameters directly influence the risk of vehicle instability caused by flooding on the link. The flood conditions in this study are assumed, so the values of h_{af} and U_{af} are also predefined. However, in practical applications of the model, these parameter values can be adjusted according to actual flood conditions. The remaining parameters in the equation represent empirical values, the specific meanings of which can be found in Appendix A.

Given l_{af} representing the proportion of the link's inundation length to its total length, a larger l_{af} amplifies the danger of flooding, thereby increasing the objective flood risk for users. To maintain the uniformity of units among the elements in the cost function and considering the inherent risk characteristics of travel time on the link, travel time is introduced as the basis for calculating flood risk. Thus, for m type users, the objective flood risk on link a and path j, denoted as r_{ima} and r_{imj} respectively, follow the expressions below:

$$r_{ima} = \left(1 + l_{af}\right) \cdot \vartheta_a \cdot t_{ima} \quad \forall i \in I, \forall m \in M_i, \forall a \in A \tag{27}$$

$$r_{imj} = \sum_{a \in A} \delta_{aj} \cdot r_{ima} \quad \forall i \in I, \forall m \in M_i, \forall j \in J_i \tag{28}$$

When the flood conditions on links within a path become more severe, the value of $\left(1 + l_{af}\right) \cdot \vartheta_a$ increases, leading to a higher r_{ima} value. Similarly, if the risk sensitivity of users in the current category increases, the value of t_{ima} will rise, further resulting in a larger r_{ima}. This indicates that the flood risk of a link is influenced by the objective flooding conditions on the link as well as the user's risk sensitivity, exhibiting a relationship akin to direct proportionality. Given the inherent uncertainty and vagueness in users' perceptions of objective flood risk, a stochastic distribution is used to capture this uncertainty. Assuming perceived path flood risk for m type users within Q_i is 'R_{imj}'. Let '$-R_{imj}$' follows a Gumbel distribution, denoted as '$-R_{imj} \sim EV(-r_{imj}, 1)$'. In this context, a larger value of r_{imj} shifts the probability density curve of R_{imj} to the right, increasing the probability of higher perceived path flood risk. Perceived flood risk among different paths is mutually independent.

(3) Path Selection Inertia

Path costs play a pivotal role in users' path judgment and selection processes. Among these costs, travel time and flood risk are inherent components that consistently influence user behavior. Additionally, subjective psychological factors can shape user decisions during these processes. When a user determines that one path, such as path 1, is acceptable and can be chosen, there will be the user's subjective psychological tendency on path 1. Judgment and selection behavior must be based on comparison between path 1 and other paths. In such cases, another path, such as path 2, serves as an anchor for comparison with path 1, and subjective tendencies toward path 1 do not extend to path 2 during the current evaluation and selection process. This asymmetry tendency in path selection is referred to as 'path selection inertia', denoted by ε_{imj}. It is worth noting that the concept of 'path selection inertia' defined in this study aims to describe the user's tendency toward a particular path in their path selection behavior and is unrelated to the commonly used concept of 'inertia' in dynamic traffic assignment. The psychological path selection inertia is incorporated into the cost function, thereby affecting users' path selection behavior. Subjective psychological perceptions of users inherently involve uncertainty and ambiguity. To capture this uncertainty, the path selection inertia of users is assumed to follow a uniform distribution. When users have higher risk sensitivity, they become more selective and cautious in their path selections. Consequently, the upper limit of path selection inertia for these users will be lower. Thus, for m type users within Q_i, the expression for path selection inertia ε_{imj} is given as follows:

$$\varepsilon_{imj} \sim Uniform\left[0, \bar{\varepsilon}_{imj}\right] \quad \forall i \in I, \forall m \in M_i, \forall j \in J_i \tag{29}$$

$$\bar{\varepsilon}_{imj} = (1 - \rho_{im}) \cdot t_{imj} \quad \forall i \in I, \forall m \in M_i, \forall j \in J_i \tag{30}$$

In real-world scenarios, flood conditions in road networks and users' subjective perceptions are highly varied. Thus, the two random variables in the cost function—perceived flood risk and path selection inertia—

may follow any distribution. Consider a probability density function curve based on perceived flood risk and path cost. Path selection inertia, reflecting the user's preference for a path, shifts this curve to the left (reducing the cost). The extent of this shift is determined by the boundary of path selection inertia, within which any shift value is possible. Consequently, this study uses a uniform distribution to represent path selection inertia. On the other hand, selecting Gumbel and uniform distributions for the two stochastic terms in the cost function ensures that the corresponding path selection probability expressions have closed-form solutions. Then, in the context of non-extreme flood, the perceived path cost for users encompasses three elements: perceived path travel time, perceived path flood risk, and path selection inertia. For m-type users, risk sensitivity consistently influences the costs associated with a path. This is because all three cost components—travel time, flood risk, and path selection inertia—are inherently associated with risk. Risk sensitivity reflects the user's attitude toward risk, thereby affecting the specific values of these cost components. A higher level of risk sensitivity leads to greater perceived travel time and flood risk. It also signifies a more cautious attitude, which results in a lower value of path selection inertia. For instance, when the risk sensitivity is equal to 1, it indicates that the user evaluates and selects paths with extreme caution and rationality, effectively eliminating path selection inertia. The perceived cost C_{imj} on the path j for m type users within Q_i satisfies:

$$C_{imj} = t_{imj} + R_{imj} - \varepsilon_{imj} \quad \forall i \in I, \forall m \in M_i, \forall j \in J_i \tag{31}$$

3. Network Equilibrium Model

3.1 Path Selection Criteria

Under non-extreme flood conditions, certain paths may be deemed too dangerous by users and thus classified as completely unacceptable. Consequently, users will not choose these unacceptable paths. Therefore, when making path selection, users will evaluate paths based on specific path selection criteria to identify acceptable and unacceptable paths. Users will then make their selections only from among their acceptable paths. Let $\bar{J}_{im}$ be the set of acceptable paths for m type users within Q_i, which is a subset of J_i. Conversely, let $\tilde{J}_{im}$ represent the set of unacceptable paths for m type users within Q_i, which is a subset of J_i.

(1) Definition and Selection of Acceptable Paths

Users determine the acceptability of paths through a comparison of path costs. During this comparison process, both perceived path travel time and perceived path flood risk are present for the paths. In the context of path selection inertia, it is not symmetrically applied to the costs of both paths during one comparison action. Instead, it is only applied to the path that the user subjectively intends to evaluate for acceptability and selection, while the other path, used as a reference for comparison, is not assigned path selection inertia. For example, for m-type users, when determining whether path j is acceptable, they compare the cost of path j with another path, denoted as path k. When m-type users subjectively assess whether path j is acceptable, they develop a psychological inclination towards path j, resulting in the application of path selection inertia to path j. In contrast, the path k being compared, does not have the user's inclination and therefore does not undergo path selection inertia. If, at this point, the cost of path j is not greater than the cost of path k, then path j is considered acceptable to m type users relative to path k. Similarly, if the user wants to determine whether path k is acceptable, path k will also receive the user's psychological inclination during this assessment, and path j will not have the user's inclination.

In other words, if the cost of path j, which includes path selection inertia, is not greater than the cost of path k, which excludes path selection inertia, then the path j is considered acceptable for m-type users and has the potential to be selected. The specific expression is as follows:

$$t_{imj} + R_{imj} - \varepsilon_{imj} \leq t_{imk} + R_{imk} \quad \forall i \in I, \forall m \in M_i, \forall j \in \bar{J}_{im}, \forall k \in J_i \tag{32}$$

This judgment method can only determine that path j is an acceptable path for m-type users, but it cannot determine that path k is unacceptable. Therefore, after m-type users have evaluated all paths, their acceptable path set may include multiple paths, each being acceptable in comparison to the others. When the acceptable path set for m-type users includes both path j and k, the following relationship holds:

$$\begin{cases} t_{imj} + R_{imj} - \varepsilon_{imj} \le t_{imk} + R_{imk} & \forall i \in I, \forall m \in M_i, \forall j,k \in \bar{J}_{im} \\ t_{imk} + R_{imk} - \varepsilon_{imk} \le t_{imj} + R_{imj} & \forall i \in I, \forall m \in M_i, \forall j,k \in \bar{J}_{im} \end{cases} \tag{33}$$

Once the acceptable path set is determined, users will select a path from within their acceptable path set. The judgment method provided by Equation (32) is used to define whether a path is considered acceptable, which essentially involves comparing the costs between two paths. The selection proportion of m type users for a particular path from the set of acceptable paths is determined by comparing that path with all the remaining paths in the acceptable set, following the judgment method represented by Equation (32). For example, for a path j in the set of acceptable paths, if path j is compared with all other remaining paths in the set using the comparison method from Equation (32), the greater the probability that path j satisfies the definition of an acceptable path, the more advantageous path j is relative to other acceptable paths, and therefore, more users will choose path j.

Let Y_{imj} represent the probability that a certain acceptable path (path j), when subjected to path selection inertia, has a cost no greater than all other acceptable paths without the path selection inertia. The expression for this probability is given as follows (the detailed derivation process is shown in Appendix D):

$$\begin{aligned} Y_{imj} &= \Pr\left(t_{imj} + R_{imj} - \varepsilon_{imj} \le t_{imk} + R_{imk}, \forall k \in \bar{J}_{im} and\ j \ne k\right) \\ &= \frac{1}{\bar{\varepsilon}_{imj}} \cdot \ln\left(1 + \frac{\left(e^{\bar{\varepsilon}_{imj}} - 1\right) \cdot e^{-(t_{imj} + r_{imj})}}{\sum_{k \in \bar{J}_{im}} e^{-(t_{imk} + r_{imk})}}\right) \\ & \qquad \forall i \in I, \forall m \in M_i, \forall j \in \bar{J}_{im} \end{aligned} \tag{34}$$

When the value of Y_{imj} is larger, it implies that for m type users, this path has a lower cost compared to other acceptable paths. Consequently, more users are likely to choose this path. Let P_{imj} represent the proportion, for this user category within this O-D pair i, that selects acceptable path j, the closed-form calculation equation for P_{imj} is obtained:

$$P_{imj} = \frac{Y_{imj}}{\sum_{k \in \bar{J}_{im}} Y_{imk}} \qquad \forall i \in I, \forall m \in M_i, \forall j \in \bar{J}_{im} \tag{35}$$

The method proposed in this paper for determining and selecting acceptable paths, as well as the method for determining unacceptable paths to be discussed later, both hinge on the asymmetric application of path selection inertia. The essence of path selection inertia lies in the user's psychological preference during the path comparison process. Since subjective psychological factors in the comparison process are inherently biased, path selection inertia is necessarily asymmetric when focusing on the micro-level comparison between paths, whether in the judgment or selection phase. However, from a more macro perspective, the user's path comparison behavior is not a one-time occurrence limited to a single path; rather, the user applies this biased comparison process to all possible paths and, after evaluating each option, ultimately selects the most satisfactory path. Thus, on a macro level, every path undergoes the influence of path selection inertia fairly, making the application of path selection inertia effectively 'symmetric' at that stage.

(2) Definition of Unacceptable Paths

The definition of acceptable paths, along with their corresponding mathematical expressions, is used to determine the assignment proportions of user demand within the acceptable path set. However, prior to path flow assignment, it is essential to establish the composition of the acceptable path set. To avoid situations where two highly dangerous paths are incorrectly classified as acceptable based on comparisons using equation (33), introduce the definition of unacceptable paths. This definition is supplemented with specific analytical expressions to facilitate judgment. Based on the judgment method provided by the unacceptable path definition, users classify paths that do not meet the unacceptable criteria as acceptable paths. This ensures a well-defined path set for subsequent assignment of user demand, which is carried out using the definition of acceptable paths. Unacceptable paths are determined through cost comparison with acceptable paths, for users, an unacceptable path invariably fails to meet the criteria defining acceptable paths entirely. When a user applies path selection inertia to a particular path (path k) and its cost remains strictly higher than that of another acceptable path (path j) without path selection inertia, path k is considered unacceptable for the user. Specifically, for m-type users within Q_i, an unacceptable path k, when compared to other acceptable paths j, must satisfy the following relationship:

$$t_{imk} + R_{imk} - \varepsilon_{imk} > t_{imj} + R_{imj} \quad \forall i \in I, \forall m \in M_i, \forall j \in \bar{J}_{im}, \forall k \in \tilde{J}_{im} \tag{36}$$

Equation (36) provides the logic for determining unacceptable paths. However, in practical applications, due to the presence of various random components in path costs, it is not feasible to directly determine whether a path is unacceptable by comparing cost values. Considering the stochastic nature of these components, use the probability of equation (36) being satisfied to identify unacceptable paths. Let Φ_{imk} represent the probability that equation (36) holds when compared to the path with the highest cost in the set of acceptable paths, and Φ_{imk} is referred to as the 'degree of unacceptability' of path k. When utilizing the maximum cost from the set of acceptable paths, due to the presence of random variables, the selection is made based on the corresponding mean values for each path. Under non-extreme flood conditions, the magnitude of the perceived path cost also reflects the level of danger associated with the path. A higher path cost indicates greater inherent risk. If the likelihood of equation (36) being satisfied is higher, it implies that the path is more dangerous compared to other paths. When the danger level of the path exceeds the user's danger tolerance, the path will be abandoned, and the user will deem it unacceptable. In this process, the parameter Φ_{imk}, which represents the degree of unacceptability, can be used to reflect the path's danger level. The specific expression for Φ_{imk} is as follows (the derivation process of Φ_{imk} is detailed in Appendix E):

$$\begin{aligned}\Phi_{imk} &= \Pr\left(t_{imk} + R_{imk} - \varepsilon_{imk} > \max\left(t_{imj} + R_{imj}\right), \forall j \in \bar{J}_{im}\right) \\ &= \frac{1}{\bar{\varepsilon}_{imk}} \cdot \frac{e^{t_{imj}+r_{imj}-t_{imk}-r_{imk}} + 1}{e^{t_{imj}+r_{imj}-t_{imk}-r_{imk}} + e^{-\bar{\varepsilon}_{imk}}} \\ &\qquad \forall i \in I, \forall m \in M_i, \forall k \notin \bar{J}_{im}\end{aligned} \tag{37}$$

The user's psychological tolerance for danger can be represented by a psychological threshold, denoted as τ_{im}, which is determined by the users' risk sensitivity: the higher the risk sensitivity, the more selective the users are in their path selection, making paths more likely to be deemed unacceptable. Then τ_{im} holds the following relationship:

$$\tau_{im} = 1 - \rho_{im} \quad \forall i \in I, \forall m \in M_i \tag{38}$$

In other words, when the unacceptability degree Φ_{imk} of path k exceeds the psychological threshold τ_{im} of m type users, path k is considered unacceptable for these users. Then for m-type users, path k is considered unacceptable when the following relationship is satisfied:

$$\Phi_{imk} \geq \tau_{im} \qquad \forall i \in I, \forall m \in M_i, \forall k \in \tilde{J}_{im} \tag{39}$$

3.2 Network Equilibrium Conditions

The network equilibrium conditions for the BST model is formulated as follows:

(a) For user category m within the same O-D pair i, the proportion of traffic on the any acceptable path is denoted as P_{imj}. This proportion, P_{imj}, is determined by the probability Y_{imj}, which represents the likelihood that the path cost with selection inertia less than or equals to the cost without selection inertia of other alternative acceptable paths.

(b) τ_{im} denotes the psychological threshold, which is directly related to the users' risk sensitivity and equals $1 - \rho_{im}$.

(c) The probability that the cost with selection inertia for user category m on any unacceptable path is strictly greater than the maximum cost without tolerance factor among all acceptable paths, is not strictly greater than the psychological threshold τ_{im}.

Utilizing these road network equilibrium conditions, the corresponding mathematical model for the network equilibrium state is as follows:

$$\begin{cases} F_{imj} > 0 \Leftrightarrow F_{imj} = P_{imj} \cdot Q_{im} & \forall i \in I, \forall m \in M_i, \forall j \in \bar{J}_{im} \\ F_{imk} = 0 \Leftrightarrow \Phi_{imk} \geq \tau_{im} & \forall i \in I, \forall m \in M_i, \forall k \in \tilde{J}_{im} \end{cases} \tag{40}$$

4. Solution Algorithm

The algorithm proposed in this paper can be abstracted into a dual-loop structure with inner and outer loops. The outer loop iterates to determine whether the acceptable and unacceptable path sets for each user type have changed and continuously updates these sets until they stabilize. The inner loop allocates the demand for different types of users based on the proposed acceptable path selection method.

The core of the algorithm involves four key components: initial anchor, flow allocation, path set update, and convergence criteria. Under non-extreme flood assumptions, users do not abandon their travel plans, meaning that for m-type users, there must be at least one acceptable path in the network. In this case, without considering path selection inertia, the path with the minimum average cost becomes the initial acceptable path for m-type users, allowing the initial anchor to be determined. For O-D pair i, m-type users have a corresponding demand Q_{im}, and the corresponding flow is allocated according to the proposed path selection probability, with the MSA method selected as the iterative algorithm for flow assignment. Under non-extreme flood disturbances, users do not abandon their travel plans, meaning that for m-type users, there must be at least one acceptable path in the network. In this case, without considering path selection inertia, the path with the minimum average cost becomes the initial acceptable path for m-type users, determining the initial anchor. For O-D pair i, m-type users have a corresponding demand Q_{im}, and the corresponding flow is allocated based on the proposed path selection probability P_{imj}, with the MSA method chosen as the iterative algorithm for flow assignment. The path update strategy involves continuously comparing each unacceptable path with the acceptable paths. If a path no longer satisfies the definition of an unacceptable path, it is added to the set of acceptable paths for m-type users, thus updating the user's path sets. When the paths for m-type users have stabilized and are no longer updated and the flows on all acceptable paths converge with MSA iterations, then the overall network convergence condition is satisfied. The detailed algorithm steps are presented as follows:

Algorithm
#1 Parameter confirmation
#1.1 Enter initial parameters
#1.1.1 $\{(Q_i \mid i \in I\}$; $\{(P_{im}, Q_{im}, \rho_{im} \mid i \in I, m \in M\}$; $\{U_{af}, l_{af}, h_{af}, t_a^0, c_a \mid a \in A\}$.
#1.1.2 Set the iteration counter $s = 1$.
#1.2 Given initial path sets
#1.2.1 Path set for O-D pair: $\{J_i \mid i \in I\}$.
#1.2.2 Path set for users: $\bar{J}_{im}^s = \emptyset, \tilde{J}_{im}^s = J_i, \forall i \in I, \forall m \in M$.
#1.2.3 Determine initial acceptable path sets: $j^* = \underset{j \in J_i}{\operatorname{argmin}}(t_{imj} + r_{imj})$, $\bar{J}_{im}^s \longleftarrow \bar{J}_{im}^s \cup \{j^*\}, \forall i \in I, \forall m \in M$.
#1.2.4 Update initial unacceptable path set: $\tilde{J}_{im}^s = J_i \setminus \bar{J}_{im}^s, \forall i \in I, \forall m \in M$.
#2 Traffic assignment for acceptable path sets
#2.1 Initial parameters
#2.1.1 Convergence threshold: ϵ. ②Initial iteration: $n = 1$. ③Maximum iterations: N.
#2.1.2 Set random initial flow: $\{f_{imj}^0 \mid i \in I, m \in M, j \in \bar{J}_{im}^s\}$. Obtain f_{ij}^0 based on the Equations (10)-(12).
#2.2 Cost components computation
Based on f_{imj}^n and f_{ij}^n, use the method of Equations (1)-(31) to compute: $\{t_{imj}, R_{imj}, \varepsilon_{imj} \mid i \in I, m \in M, j \in \bar{J}_{im}^s\}$.
#2.3 Flow updates
#2.3.1 Compute the path selection probability P_{imj}^n using Equations (34)-(35).
#2.3.2 Determine the new path flow x_{imj}^n.
#2.3.3 Updates the path flow: $f_{imj}^n = \left(1 - \frac{1}{n}\right) \cdot f_{imj}^{n-1} + \frac{1}{n} \cdot x_{imj}^n$. Then obtain f_{ij}^n based on the Equations (10)-(12).
#2.4 Convergence judgment

If $\left|f_{ij}^{n}-f_{ij}^{n-1}\right|<\epsilon$ or $n=N$, it converges and enters (#3). If it does not converge, let $n=n+1$ and return to (#2.2).

#3 Path set updates

#3.1 Compute the degree of unacceptability: $k^{*}=\underset{k\in\tilde{J}_{im}^{s}}{\operatorname{argmin}}\left(Equation(37)\right),\forall i\in I,\forall m\in M.$

#3.2 Convergence judgment: If $\Phi_{imk^{*}}<\tau_{im},\forall i\in I,\forall m\in M$, let $s=s+1$, $\bar{J}_{im}^{s}\longleftarrow\bar{J}_{im}^{s-1}\cup\{k^{*}\}$, $\tilde{J}_{im}^{s}=J_{i}\setminus\bar{J}_{im}^{s},\forall i\in I,\forall m\in M$, and return to (#2). If $\Phi_{imk^{*}}\geq\tau_{im},\forall i\in I,\forall m\in M$, the overall algorithm converges and output the results.

5. Numerical Results

5.1 Case 1

5.1.1 Settings

This case employs the Nguyen and Dupuis network as the traffic network for the application of BST model, as illustrated in Figure 1. The network comprises 13 nodes and 19 links. And a subset of links in this network is affected by non-extreme flood, represented by the blue regions. In this network, there are two O-D pairs, and the demand for each O-D pair follows a normal distribution. Furthermore, users within each O-D pair are classified into different categories based on their risk sensitivity. The specific demand distribution characteristics and user classification parameters can be found in Table 1.

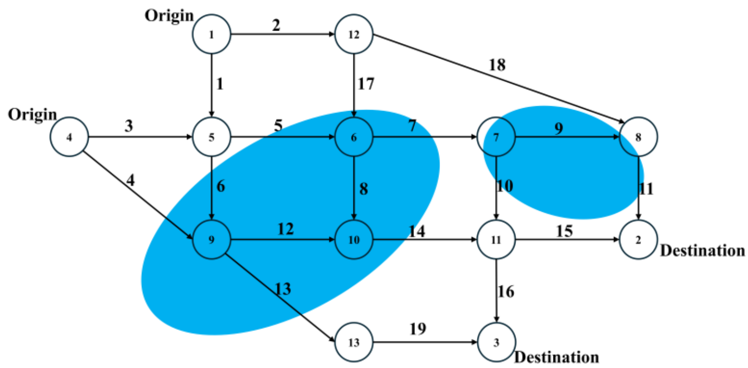

Fig. 1. The Nguyen and Dupuis network with two distinct flooded regions

Table 1

Characteristics of O-D pairs and user classification features

O-D pair	Mean *[pcu/hour]*	Standard deviation	User type Q_{im}	Proportion P_{im}	Risk sensitivity ρ_{im}
(1, 3)	700	140	Q_{11}	0.2	0.3
			Q_{12}	0.6	0.5
			Q_{13}	0.2	0.7
(4, 2)	400	80	Q_{21}	0.3	0.5
			Q_{22}	0.7	0.7

Table 2 provides information on the flood characteristics of links affected by flooding, where all links have a free-flow travel time of 3 and a capacity of 500. Considering the non-extreme flooding background in this paper, the flood parameter settings on each link will not introduce extreme risks that would lead users to abandon their travel plans. To calculate the objective risk associated with flooding on the links, it is necessary to provide characteristic parameters such as the average length and height of vehicles on the links, as shown in Table 3. Table 4 details the paths corresponding to different O-D pairs and the links constituting each path. In the calculations, parameters for the BPR function are involved, with β set to 0.15 and λ set to 4.

Table 2

Values of link characteristic parameters under flood conditions

Link number	l_{af} *(%)*	h_{af} *(m)*	U_{af} $(m\cdot s^{-1})$	Link number	l_{af} *(%)*	h_{af} *(m)*	U_{af} $(m\cdot s^{-1})$
1	0	0	0	11	70	0.5	6
2	0	0	0	12	100	0.3	5

3	0	0	0	13	70	0.4	6
4	20	0.4	4	14	30	0.3	5
5	70	0.3	5	15	0	0	0
6	80	0.6	6	16	0	0	0
7	60	0.2	5	17	10	0.3	4
8	100	0.3	5	18	0	0	0
9	100	0.3	5	19	0	0	0
10	50	0.6	5				

Table 3
Values of Vehicle Parameters on the Links

w_1	w_2	$h_c\ (m)$	$g\ (m \cdot s^{-2})$	$l_c\ (m)$	$\rho_c\ (kg \cdot m^{-3})$	$\rho_f\ (kg \cdot m^{-3})$	R_f
0.35	-0.45	1.6	9.8	5	190	1000	0.55

Table 4
Path and link sequences

O-D pair	Path number	Link sequence
(1, 3)	1	1-6-13-19
	2	2-17-8-14-16
	3	2-17-7-10-16
	4	1-6-12-14-16
	5	1-5-7-10-16
	6	1-5-8-14-16
(4, 2)	7	3-5-7-9-11
	8	3-5-7-10-15
	9	3-5-8-14-15
	10	3-6-12-14-15
	11	4-12-14-15

5.1.2 Results

The determination of acceptable path sets for users of different categories is not an instantaneous process, it involves dynamic comparisons over iterations to eventually confirm their respective acceptable path sets, leading to equilibrium on the acceptable path sets. The iterative evolution of acceptable path sets for a total of five user categories within the two O-D pairs is presented in Table 5.

Table 5
Dynamic Evolution Process of Acceptable Path Sets

Evolution Process	The acceptable path set of user type Q_{11}	The acceptable path set of user type Q_{12}	The acceptable path set of user type Q_{13}	The acceptable path set of user type Q_{21}	The acceptable path set of user type Q_{22}
The Initial State	$\emptyset$	$\emptyset$	$\emptyset$	$\emptyset$	$\emptyset$
As the Algorithm Iterations Increase	1	1	1	11	11
	1, 3	1, 3	1, 3	11, 8	11, 8
	1, 3, 5	1, 3, 5	1, 3	11, 8, 9	11, 8
	1, 3, 5, 2,	1, 3, 5, 2,	1, 3	11, 8, 9, 10	11, 8
	1, 3, 5, 2, 6	1, 3, 5, 2, 6	1, 3	11, 8, 9, 10	11, 8
Complete Equilibrium in the Road Network	1, 3, 5, 2, 6, 4	1, 3, 5, 2, 6, 4	1, 3	11, 8, 9, 10	11, 8

Figures 2 and 3 illustrate the corresponding dynamic iteration process of acceptable paths for users within two O-D pairs. Then a clear depiction of the users' path selection process during dynamic iteration emerges. The information in Figure 2 and Figure 3 clearly illustrates the dynamic selection process. In each iteration, users of the corresponding categories compare the remaining non-acceptable paths in the network. They judge and choose whether to add an acceptable path. This process continues until there is no further change in the acceptable path set for all users. Then users are assigned only on these acceptable paths, satisfying the principles of network equilibrium conditions of the proposed model. In each new path selection process, users consistently demonstrate their instinct to avoid risks. Taking the example of the three categories of users within the O-D pair (1, 3), in the first two iterations of Figure 2, all three categories of users chose paths 1 and 3 as their acceptable paths. This is because, among all paths, only paths 1 and 3 can avoid flooded links 8 and 12, where the flood situation is most dangerous. In the next iteration, the Q_{13} users no longer add new acceptable paths. Only the Q_{11} and Q_{12} users choose to add new acceptable paths. This is because Q_{13} users are more sensitive to risks, and for them, the remaining paths are considered too dangerous. Therefore, they do not accept new paths. This phenomenon reflects the realistic behavior of users with high-risk sensitivity in the context of a flood disaster. Observing Figure 3 and Table 5, it illustrates the path selection process for users within the O-D pair (4, 2). For all users in the O-D pair (4, 2), reaching the destination implies crossing both the left and right flooded areas. No matter which paths it is, each path includes links submerged in the left flood zone. In this situation, the safest approach is to prioritize paths with minimal impact from the left flood zone, meaning selecting links with the least danger among those submerged by the left flood. Simultaneously, users aim to choose links unaffected by the right flood zone as much as possible. Based on this consideration, the optimal choice for users in the O-D pair (4, 2) is expected to be Path 11, as it minimizes exposure to the left flood zone while avoiding the most dangerous links. The model's simulation results align with this optimal path selection strategy. The suboptimal choice would be Path 8, as it circumvents the riskier links (8, 9, and 12) in the left flood zone. When further selecting additional acceptable paths, users' risk sensitivity comes into play. The Q_{22} users, with higher risk sensitivity, chooses not to accept the remaining high-risk paths. Consequently, their acceptable paths remain Paths 11 and 8. In contrast, the Q_{21} users, less concerned about risks, can accept even riskier paths, such as Paths 9 and 10. These results strongly demonstrate the model's capability to effectively simulate users' dynamic path selection behavior in the context of a flood disaster.

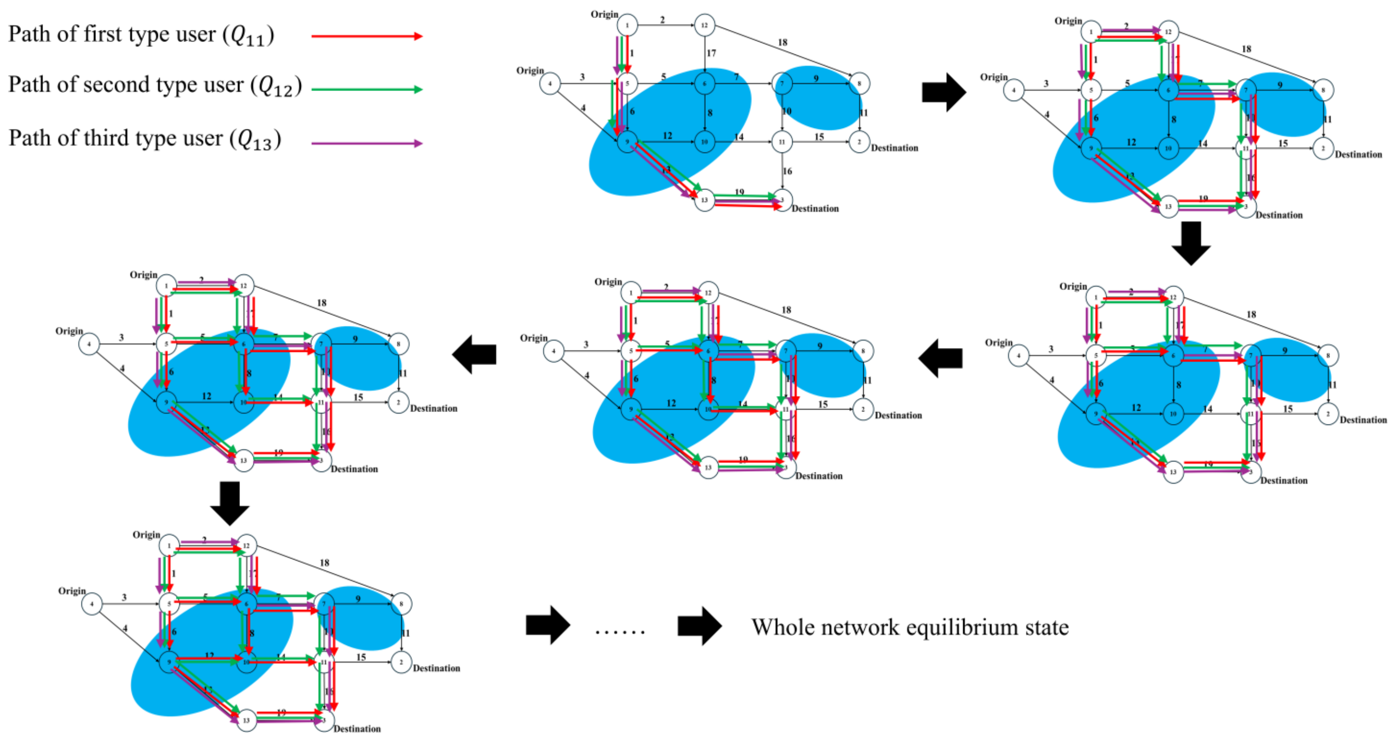

Fig. 2. Dynamic Evolution of Acceptable Path Set for Users within O-D Pair (1, 3)

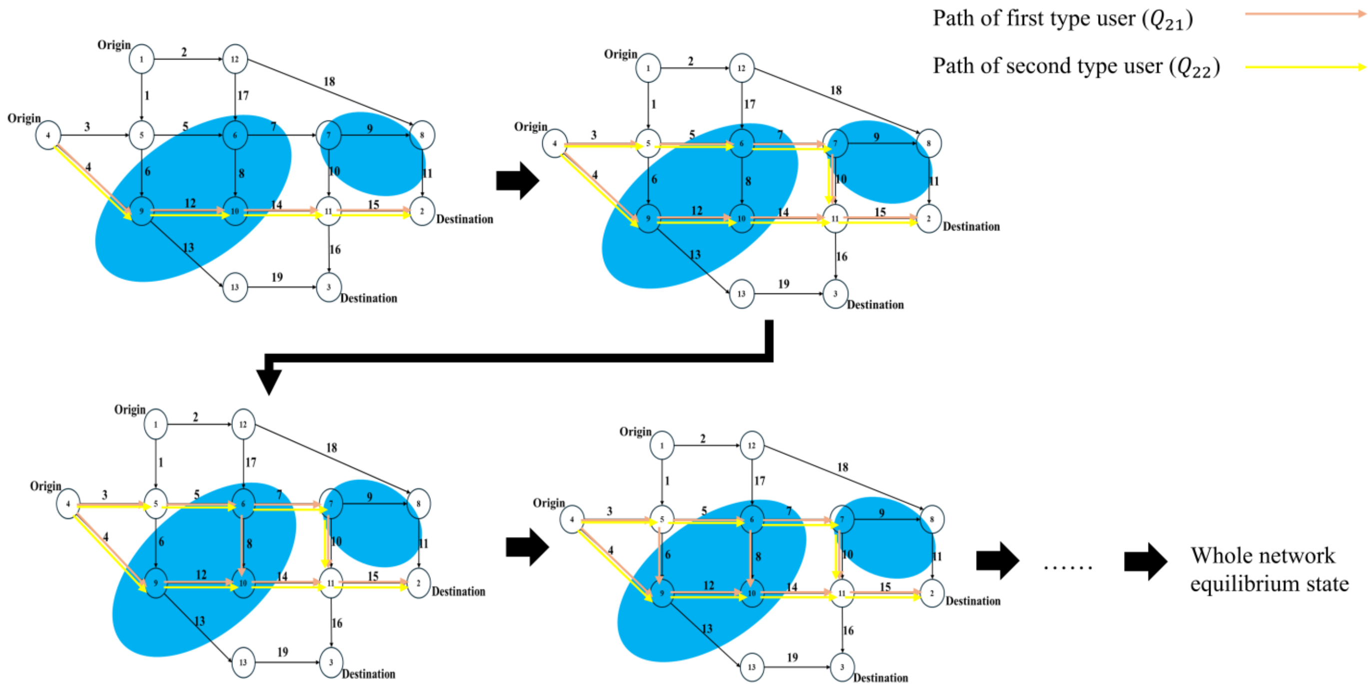

Fig. 3. Dynamic Evolution of Acceptable Path Set for Users within O-D Pair (4, 2)

Based on Table 5, users Q_{11} and Q_{13} began the iterative process of determining their acceptable path sets, starting with Path 1 as their first acceptable path. During the first judgment, Path 3 was included in the acceptable path set for both Q_{11} and Q_{13}. In the second judgment, Q_{11} added Path 5 to its acceptable path set, whereas Q_{13} did not accept any new paths. Figure 4 illustrates the path cost composition for both user types during the first and second judgments. For simplicity, the random variables representing perceived flood risk (R_{imj}) and path selection inertia (ε_{imj}) are denoted by r_{imj} and $E[\varepsilon_{imj}]$, respectively. It can be observed that the acceptable path costs for Q_{13} are consistently higher than those for Q_{11} during both the first and second judgments. This discrepancy arises from the higher risk sensitivity of Q_{13}, leading them to perceive greater path costs, including travel time and flood risk. In the first judgment, apart from Path 1 (already classified as acceptable), Path 3 had the lowest cost among the remaining paths, significantly lower than the cost of Path 1. Thus, both Q_{11}, with lower risk sensitivity, and Q_{13}, with higher risk sensitivity, selected Path 3 as their new acceptable path in this round. Following the same logic, during the second judgment, Path 5 had the lowest cost among the remaining paths that were not yet acceptable. Users then evaluated whether Path 5 could be included in their acceptable path sets. For Q_{11}, Path 5 had a cost 1.1 units higher than Path 3, but this increase in cost was within their tolerance, prompting them to accept Path 5. The higher cost represents additional risk, but due to Q_{11}'s lower risk sensitivity, they were willing to accept Path 5 as a new acceptable path. For Q_{13}, the cost difference between Path 5 and Path 3 was only 0.4 units—substantially smaller than for Q_{11}—yet Q_{13} rejected Path 5. This is because Q_{13}'s high risk sensitivity renders even small increases in risk cost unacceptable, leading them to classify Path 5 as an unacceptable path. This behavior reflects the model's ability to effectively simulate the path selection behavior of users with varying risk sensitivities in a flood scenario. As shown in Figure 5, after Q_{13} finalized their acceptable path set as Path 1 and Path 3, they began making choices exclusively within this set. For clarity, the path costs are represented by t_{imj}, r_{imj}, and ε_{imj}. It can be observed that through iterative path selection, the flow no longer changes after a certain point, indicating that Q_{13}'s demand achieves equilibrium within their acceptable path set.

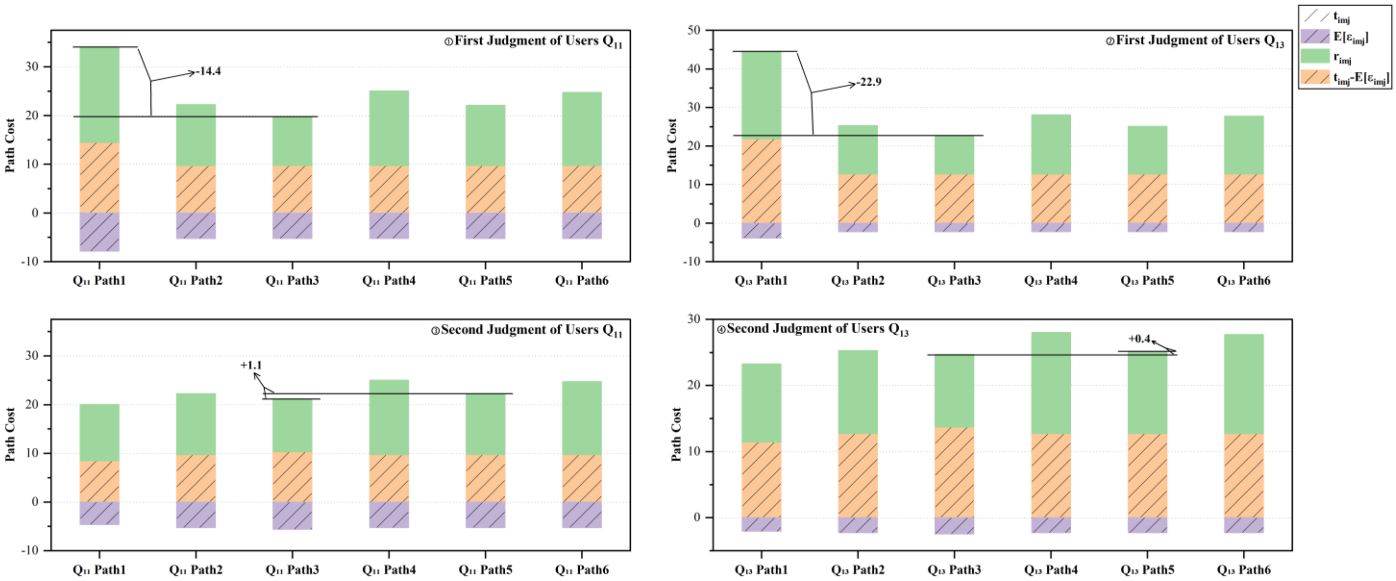

Fig. 4. Path costs for users Q_{11} and Q_{13} during the first and second acceptable path judgments.

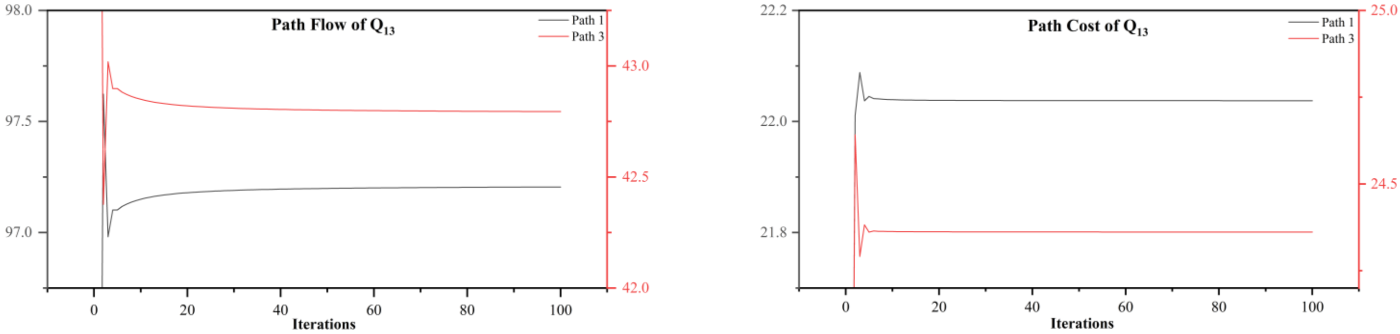

Fig. 5. Changes in flow and cost within the acceptable path set of users Q_{13} during MSA iterations.

Once all user types across all O-D pairs have determined their acceptable path sets, they proceed to make path choices within the same network until the entire network reaches an equilibrium state. Path flows are iteratively reassigned until reaching equilibrium using the MSA algorithm. To illustrate network convergence through changes in path flow, the gap function method is applied to evaluate the convergence of the 11 paths in the network. The path flow-based gap function is defined as follows:

$$Relative\ Flow\ Gap_k^n = \frac{f_k^n - f_k^{n-1}}{f_k^{n-1}} \tag{41}$$

where k represents the path, and f_k^n denotes the flow on path k at the n-th iteration. This function quantifies the difference in flow assignments for each path between successive iterations. As iterations progress, the gap values approaching zero indicate stabilizing path flow assignments and that the network is nearing equilibrium. Figure 6 shows the flow gap changes for all 11 paths across iterations. The results demonstrate that as iterations increase, the flow gap values for all paths converge to zero, signifying that the network has reached equilibrium after users finalize their acceptable path sets and iteratively select paths.

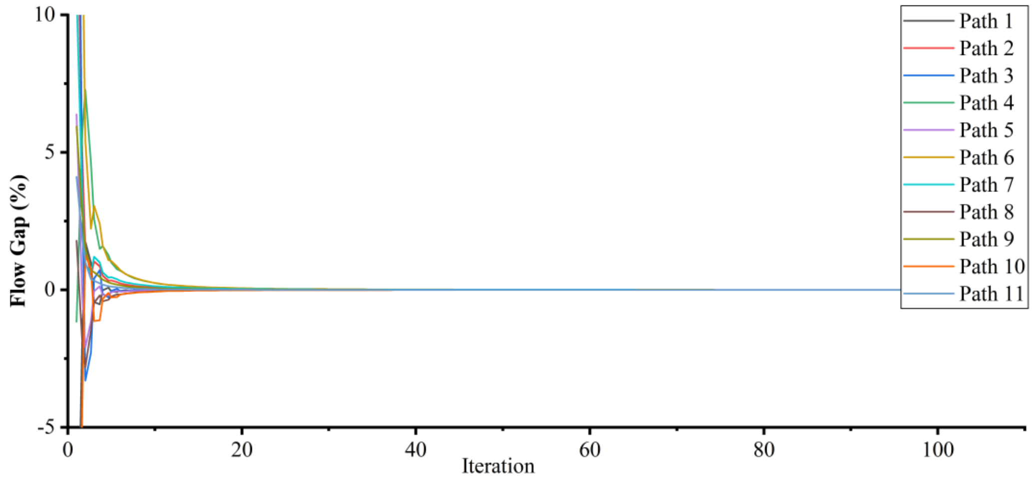

Fig. 6. Fluctuations in relative path flow gaps across iterations.

5.2 Case 2

5.2.1 Settings

To validate the effectiveness of the model in a larger real-world network, the Sioux-Falls network was utilized for traffic network analysis and simulation. The Sioux-Falls network consists of 24 nodes and 76 links, with its structure illustrated in Figure 7. The blue shaded area represents regions submerged by non-extreme flooding. The characteristics of the corresponding links, including free-flow travel time, link capacity, flood depth, and flood flow velocity, are detailed in Table 6. For simplicity and ease of comparison, only the flood conditions for the submerged links are shown in Table 6, the capacity of all links is set to 80, and the free-flow travel time is set to 10.

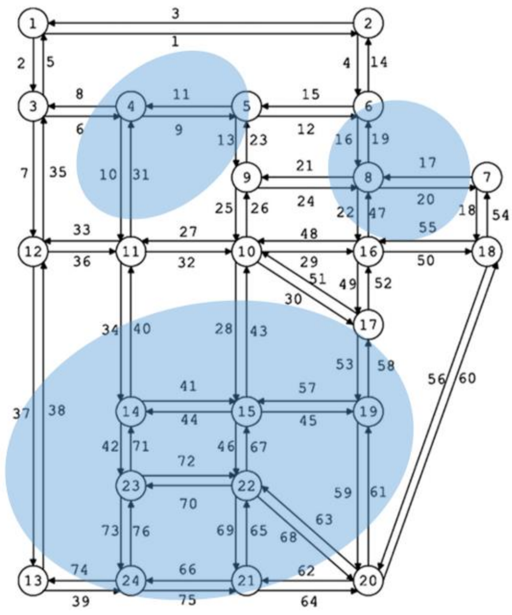

Fig. 7. The Sioux-falls network with three distinct flooded regions

Table 6
Values of link characteristic parameters under flood conditions

Link number	t_a^0	c_a	l_{af}	h_{af}	U_{af}	Link number	t_a^0	c_a	l_{af}	h_{af}	U_{af}
6	10	80	0.3	0.2	3	44	10	80	1	0.6	6
8	10	80	0.3	0.2	3	45	10	80	1	0.5	5
9	10	80	1	0.5	6	46	10	80	1	0.6	7
10	10	80	0.8	0.4	5	47	10	80	0.9	0.3	4
11	10	80	1	0.5	6	53	10	80	1	0.3	4
13	10	80	0.5	0.2	4	57	10	80	1	0.5	5
16	10	80	1	0.4	5	58	10	80	1	0.3	4
17	10	80	0.9	0.5	6	59	10	80	0.7	0.4	4

19	10	80	1	0.4	5	61	10	80	0.7	0.4	4
20	10	80	0.9	0.5	6	63	10	80	0.8	0.5	6
21	10	80	0.3	0.3	3	65	10	80	1	0.5	5
22	10	80	0.8	0.3	4	66	10	80	1	0.3	3
23	10	80	0.1	0.2	4	67	10	80	1	0.6	7
24	10	80	0.3	0.3	3	68	10	80	0.8	0.5	6
28	10	80	0.7	0.4	5	69	10	80	1	0.5	5
31	10	80	0.8	0.4	5	70	10	80	1	0.6	7
34	10	80	0.5	0.5	5	71	10	80	1	0.5	6
37	10	80	0.4	0.3	3	72	10	80	1	0.6	7
38	10	80	0.4	0.3	3	73	10	80	1	0.3	4
40	10	80	0.5	0.5	5	74	10	80	0.3	0.3	3
41	10	80	1	0.6	6	75	10	80	1	0.3	3
42	10	80	1	0.5	6	76	10	80	1	0.3	4
43	10	80	0.7	0.4	5						

The empirical parameter values for vehicles on the links are consistent with those in Table 3. It is assumed that the demand for O-D pair follows a normal distribution, encompassing three types of users with different risk sensitivities, whose distribution characteristics are shown in Table 7. To better demonstrate the model's ability to simulate users' path selection behavior under non-extreme flooding conditions, as well as to highlight the correlation between the acceptable path sets, user risk sensitivity, and flood conditions, 100 randomly generated paths for the O-D pair are provided for model validation. The specific paths and the nodes connecting these paths are shown in Table 8. In the calculations, parameters for the BPR function are involved, with β set to 0.15 and λ set to 4.

Table 7

Characteristics of O-D pair and user classification features

O-D pair	Mean *[pcu/hour]*	Standard deviation	User type Q_{im}	Proportion P_{im}	Risk sensitivity ρ_{im}
(1, 20)	100	20	Q_{11}	0.2	0.2
			Q_{12}	0.5	0.5
			Q_{13}	0.3	0.9

Table 8

Path and node sequences

No. Path	Seq. Node	No. Path	Seq. Node	No. Path	Seq. Node	No. Path	Seq. Node
1	[1,3,4,11,14,23,22,20]	**26**	[1,3,12,11,10,15,22,21,20]	**51**	[1,3,12,13,24,21,22,20]	**76**	[1,3,4,11,10,17,19,15,22,21,20]
2	[1,3,12,11,14,23,22,20]	**27**	[1,3,12,11,14,15,19,20]	**52**	[1,3,12,11,14,23,24,21,22,20]	**77**	[1,3,12,11,10,17,19,15,22,21,20]
3	[1,3,4,5,9,10,15,22,20]	**28**	[1,3,12,11,14,15,22,21,20]	**53**	[1,3,4,5,6,8,7,18,20]	**78**	[1,3,4,5,9,10,15,14,23,24,21,20]
4	[1,3,4,11,10,15,22,20]	**29**	[1,3,4,5,9,10,16,17,19,20]	**54**	[1,3,4,5,6,8,16,18,20]	**79**	[1,3,4,5,9,10,15,14,23,22,21,20]
5	[1,3,4,11,14,15,22,20]	**30**	[1,3,4,11,10,16,17,19,20]	**55**	[1,3,4,5,6,8,16,17,19,15,22,20]	**80**	[1,3,4,11,10,15,14,23,24,21,20]
6	[1,3,12,11,10,15,22,20]	**31**	[1,3,12,11,10,16,17,19,20]	**56**	[1,3,4,5,9,8,7,18,20]	**81**	[1,3,4,11,10,15,14,23,22,21,20]
7	[1,3,12,11,14,15,22,20]	**32**	[1,3,4,5,9,10,17,19,15,22,20]	**57**	[1,3,4,5,9,8,16,18,20]	**82**	[1,3,12,11,10,15,14,23,24,21,20]
8	[1,3,4,5,9,10,17,19,20]	**33**	[1,3,4,11,10,17,19,15,22,20]	**58**	[1,3,4,5,9,8,16,17,19,15,22,20]	**83**	[1,3,12,11,10,15,14,23,22,21,20]
9	[1,3,4,11,10,17,19,20]	**34**	[1,3,12,11,10,17,19,15,22,20]	**59**	[1,3,4,5,9,10,16,18,20]	**84**	[1,3,4,5,9,10,11,14,23,24,21,20]
10	[1,3,12,11,10,17,19,20]	**35**	[1,3,4,5,9,10,15,14,23,22,20]	**60**	[1,3,4,5,9,10,16,17,19,15,22,20]	**85**	[1,3,4,5,9,10,11,14,23,22,21,20]
11	[1,2,6,8,16,17,19,20]	**36**	[1,3,4,11,10,15,14,23,22,20]	**61**	[1,3,4,11,10,16,18,20]	**86**	[1,3,4,5,9,10,11,14,15,19,20]
12	[1,3,4,11,14,23,24,21,20]	**37**	[1,3,12,11,10,15,14,23,22,20]	**62**	[1,3,4,11,10,16,17,19,15,22,20]	**87**	[1,3,4,5,9,10,11,14,15,22,21,20]
13	[1,3,4,11,14,23,22,21,20]	**38**	[1,3,4,5,9,10,11,14,23,22,20]	**63**	[1,3,12,11,10,16,18,20]	**88**	[1,2,6,5,9,10,17,19,20]
14	[1,3,12,13,24,21,20]	**39**	[1,3,4,5,9,10,11,14,15,22,20]	**64**	[1,3,12,11,10,16,17,19,15,22,20]	**89**	[1,2,6,8,9,10,17,19,20]
15	[1,3,12,11,14,23,24,21,20]	**40**	[1,3,4,11,12,13,24,21,20]	**65**	[1,2,6,8,9,10,15,22,20]	**90**	[1,2,6,8,16,10,17,19,20]
16	[1,3,12,11,14,23,22,21,20]	**41**	[1,3,4,11,14,23,22,15,19,20]	**66**	[1,2,6,8,16,10,15,22,20]	**91**	[1,3,4,5,6,8,9,10,17,19,20]
17	[1,3,4,5,6,8,16,17,19,20]	**42**	[1,3,12,11,14,23,22,15,19,20]	**67**	[1,3,4,5,6,8,9,10,15,22,20]	**92**	[1,3,4,5,6,8,16,10,17,19,20]
18	[1,3,4,5,9,8,16,17,19,20]	**43**	[1,3,4,11,10,9,8,16,17,19,20]	**68**	[1,3,4,5,6,8,16,10,15,22,20]	**93**	[1,3,4,5,9,8,16,10,17,19,20]
19	[1,3,4,5,9,10,15,19,20]	**44**	[1,3,12,11,10,9,8,16,17,19,20]	**69**	[1,3,4,5,9,8,16,10,15,22,20]	**94**	[1,3,12,11,4,5,9,10,15,22,20]
20	[1,3,4,5,9,10,15,22,21,20]	**45**	[1,2,6,5,9,10,15,22,20]	**70**	[1,3,4,5,9,10,15,22,23,24,21,20]	**95**	[1,3,4,11,14,15,10,17,19,20]
21	[1,3,4,11,10,15,19,20]	**46**	[1,2,6,8,7,18,20]	**71**	[1,3,4,11,10,15,22,23,24,21,20]	**96**	[1,3,12,11,14,15,10,17,19,20]
22	[1,3,4,11,10,15,22,21,20]	**47**	[1,2,6,8,16,18,20]	**72**	[1,3,4,11,14,15,22,23,24,21,20]	**97**	[1,2,6,5,9,8,16,17,19,20]
23	[1,3,4,11,14,15,19,20]	**48**	[1,2,6,8,16,17,19,15,22,20]	**73**	[1,3,12,11,10,15,22,23,24,21,20]	**98**	[1,2,6,5,9,10,15,19,20]
24	[1,3,4,11,14,15,22,21,20]	**49**	[1,3,4,11,14,23,24,21,22,20]	**74**	[1,3,12,11,14,15,22,23,24,21,20]	**99**	[1,2,6,5,9,10,15,22,21,20]
25	[1,3,12,11,10,15,19,20]	**50**	[1,3,12,13,24,23,22,20]	**75**	[1,3,4,5,9,10,17,19,15,22,21,20]	**100**	[1,2,6,8,7,18,16,17,19,20]

5.2.2 Results

To demonstrate that all paths in the network have reached equilibrium, given the large number of paths, it is not easy to directly observe the fluctuations in every path flow with each iteration. Therefore, a gap function based on path flow is used to measure the convergence of the network system. Unlike in Case 1, the large number of paths here necessitates constructing the flow gap function for overall paths. The corresponding function is as follows:

$$Flow\ Gap = \sum_{k}^{100} \left| \frac{f_k^n - f_k^{n-1}}{f_k^{n-1}} \right| \tag{42}$$

where f_k^n represents the flow of path k during the n-th iteration, and f_k^{n-1} refers to the flow of path k in the previous iteration. Figure 8 shows the overall fluctuation of the flow gap across all paths with each iteration. It can be observed that as the iterations progress, the overall gap in flow for all paths approaches 0, indicating that the flow assignment across all paths has reached a stable state, and the network has achieved equilibrium. The fact that the paths have reached equilibrium demonstrates that the model can effectively simulate the traffic flow assignment in the network under the influence of non-extreme flooding. This helps to determine the usage of various paths within the network under such conditions, providing valuable insights for managers to optimize and manage the network accordingly.

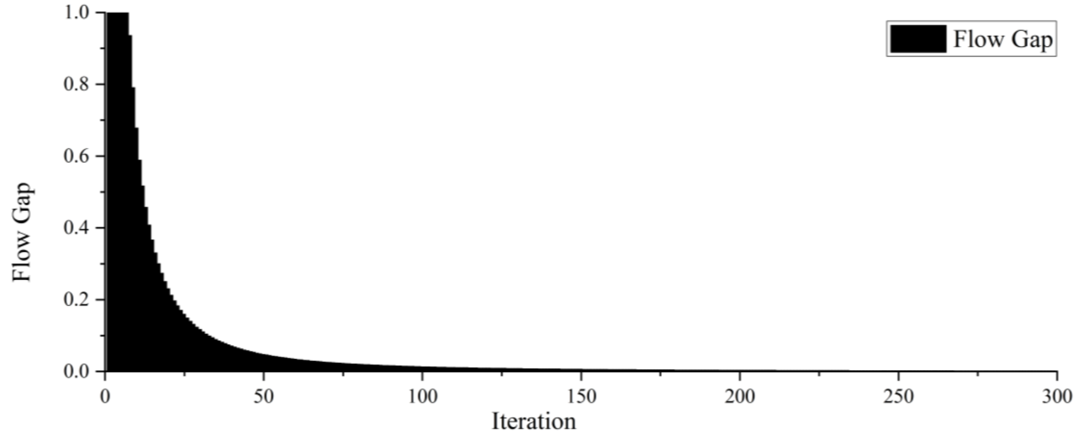

Fig. 8. Fluctuation of the flow gap of overall paths with each iteration.

Table 9 illustrates the number of acceptable paths for different types of users when the network reaches equilibrium, along with the elements contained in the sets of acceptable paths. Q_{11} users have 50 acceptable paths, Q_{12} users have 33, while Q_{13} users have only one acceptable path. The variation in the number of acceptable paths for different user types clearly reflects the impact of risk sensitivity on the determination of acceptable paths. For Q_{11} users, who have low risk sensitivity, this indicates that they are the least concerned with flood-related risks among the three types of users. As a result, more paths are considered acceptable, and these users can choose from a larger set of paths. In contrast, Q_{12} users have a higher risk sensitivity than Q_{11} users, leading to a reduction in the number of acceptable paths. The increased risk sensitivity means that Q_{12} users are more focused on potential risks, making them more selective in their path selections. Therefore, paths that are acceptable to Q_{11} users may be deemed unacceptable by Q_{12} users. For example, the paths 97, 16, and 28, which are considered acceptable for Q_{11} users, are deemed unacceptable for Q_{12} users. Q_{13} users have an even higher level of risk sensitivity, reaching an extreme level. These users are particularly concerned with flood risks along the paths, making their evaluation of paths highly stringent. Consequently, despite having 100 available routes, only one is deemed acceptable by Q_{13} users. This outcome effectively demonstrates that the proposed model can be successfully applied to scenarios where large networks are subjected to non-extreme flood disturbances. It provides a valuable tool for simulating and analyzing users' path selection behavior, enabling network managers to assess and predict the usage of various paths under different non-extreme flood conditions, thereby supporting the operation and maintenance of the network under such scenarios.

Table 9
Number of acceptable paths for different types of users and corresponding acceptable path sets

User category	Number of acceptable paths	Composition of the acceptable path set
Q_{11}	50	{63,14,47,61,46,10,59,31,88,25,40,6,9,51,50,57,11,30,26,56,54,27,89,98,7,2,45,15,53,8,21,4,90,97,16,28,99,29,44,22,23,65,1,5,100,19,12,34,3,66}
Q_{12}	33	{63,14,47,61,46,10,59,31,88,25,40,6,9,51,50,57,11,30,26,56,54,27,89,98,7,2,45,15,53,8,21,4,90}
Q_{13}	1	{63}

Figure 9 presents a schematic diagram of certain paths in the traffic road network. When combined with the path composition of the user-acceptable path sets in Table 9, it further illustrates how risk sensitivity influences users' path selection behavior under non-extreme flood conditions. For all three types of users, Path 63 is unanimously chosen as the first acceptable path. Even for Q_{13} users, who are particularly risk-sensitive and only accept a single path, Path 63 remains the sole choice. This is because Path 63 is the only path among the 100 alternatives that is unaffected by flooding. As shown in Figure 9, Path 63 avoids all three flood-affected areas in the network, making it a risk-free path and the preferred choice for all user types. For Q_{13} users, any path other than Path 63 is associated with varying degrees of flood risk, and thus no other path is deemed acceptable. Q_{12} users, with lower risk sensitivity, find certain low-risk paths acceptable. For instance, Paths 14 and 47 are identified by Q_{12} users as acceptable after Path 63. Although these paths pass through flood-affected areas, they only traverse the edges of one flooded region. While these paths involve some level of flood risk, which makes them unacceptable to Q_{13} users, the lower risk is acceptable to Q_{12} users. Compared to Paths 47 and 14, Path 61 also crosses only one flooded region but is considered acceptable by Q_{12} users after Path 47. This is because Path 61 passes closer to the core of the flooded area, making the risk greater compared to Path 47, which stays near the outskirts of the flooded region. Therefore, Path 61 is accepted by Q_{12} users only after Path 47.

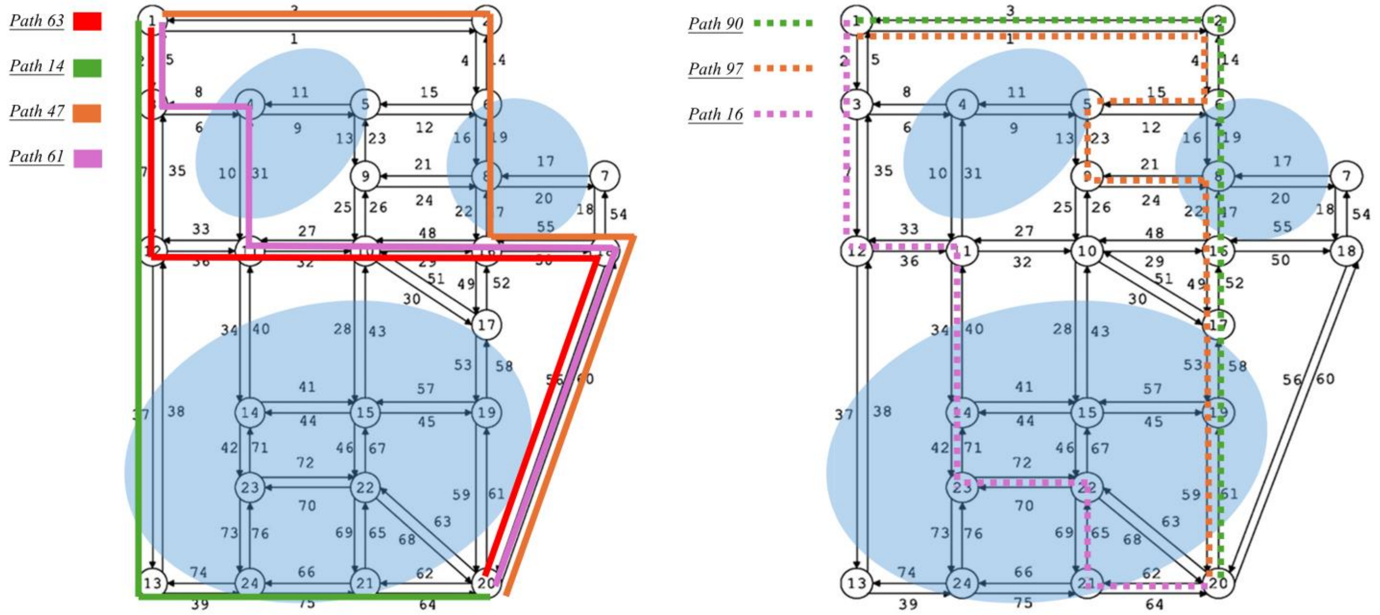

Fig. 9. Diagram of paths corresponding to some certain paths in the traffic network.

Q_{11} users, with even lower risk sensitivity than Q_{12} users, accept paths that are deemed unacceptable by Q_{12} users. Path 97 is the threshold where paths become acceptable for Q_{11} users but not for Q_{12} users. Path 90 is acceptable to both Q_{11} and Q_{12}. Path 97 and Path 90 share many of the same links, but Path 97 avoids Link 16 by taking a detour via Links 15, 13, and 24. Although Path 97 bypasses the flood-affected Link 16, it still passes through Link 24, which is also flooded. More importantly, the detour significantly increases travel time, and under flood conditions, longer travel time correlates with greater risk. Therefore, despite its similarity to Path 90, Path 97's overall risk leads to its rejection by Q_{12} users, while it remains acceptable to the less risk-sensitive Q_{11} users. Path 16, which passes through the core of the flooded region, poses a risk that is unacceptable to highly risk-sensitive user types. However, Q_{11} users, with their low-risk sensitivity, are willing to select Path 16 as an acceptable option. The composition of acceptable paths for users with varying risk sensitivities and the selection process demonstrates that the proposed model effectively simulates users' path selections under different flood conditions. This model can aid in analyzing and predicting path usage during actual non-extreme flood events, thus enhancing the efficiency of road network emergency management.

6. Conclusion

This paper develops a network equilibrium model where the path selection behavior is derived considering multiple issues under non-extreme flooding scenarios, including travel time variability, flooding risk, and path selection inertia. Travelers are divided into multiple classes with different risk-taking attitudes, while paths are grouped into acceptable and unacceptable sets using generalized path costs. Results demonstrate the model's efficacy in simulating path selection behavior among users with different risk sensitivities under non-extreme flood conditions. By incorporating a cost function comprising two stochastic terms, the model captures both objective costs and subjective psychological factors influencing user decisions. Particularly, the acquisition of perceived path time is conducted on a link-based operation basis, effectively reflecting the risk characteristics of travel time. The introduction of the concepts of 'acceptable paths' and 'unacceptable paths' in the BST model effectively simulates users' instinct to mitigate risks under flood conditions, wherein users select the safest paths with minimal flood impact and reflecting the logical judgment process during path selection. The proposal of new network equilibrium conditions in the BST model ensures the dynamic adaptation of the acceptable path set based on user risk sensitivity, which demonstrates the role of risk sensitivity in user path selection. The introduction of the BST model presents a novel approach where the path selection set dynamically adjusts with both objective environmental factors and user subjective elements, thereby facilitating the development and application of STA models in flood contexts. Moreover, this approach holds potential for application in research concerning other disaster scenarios. While the BST model proposed in this paper accounts for the heterogeneity of user risk sensitivity, it is acknowledged that user heterogeneity in real-world scenarios is more complex, suggesting room for improvement and further development in this direction.

7. Statements and Declarations

The authors did not receive support from any organization for the submitted work. The authors have no competing interests to declare that are relevant to the content of this article.

Appendix

A. The Notations Employed in the Paper

Notation	Definition	Notation	Definition
A	Set of links in the network	I	Set of O-D pairs in the network
J_i	Set of paths between O-D pair i	M_i	Set of categories of users within the O-D pair i
δ_{aj}	Variable that equals 1 if link a is part of path j and equals 0 otherwise	V_a	Stochastic flow of link a
C_a	Capacity of link a	F_{ij}	Stochastic flow of path j between O-D pair i
F_{imj}	Stochastic flow of path j between O-D pair i	Q_i	Stochastic total O-D flow between O-D pair i
Q_{im}	Demand for different categories of uses within the same O-D pair i	T_{ij}	Stochastic travel time on the path j which serves the O-D pair i
T_a	Stochastic travel time on the link a	P_{im}	The proportion of demand for different categories users Q_{im} to Q_i within the same O-D pair i
ρ_{im}	Sensitivity and aversion levels to risk for the specific user type m within the same O-D pair i	ϑ	The degree of risk for a vehicle to lose stability
U_{af}	Flood velocity on the link a	U_{ac}	The critical velocity of vehicle instability on the

			link a
w_1, w_2	The parameters related to the vehicle appearance, tire type and roughness of the road surface	h_{af}	Flood depth on the link a
ρ_f	The density of the flood water	h_c	Average height of the vehicle
l_c	The average length of the vehicle	ρ_c	The average density of the vehicle
g	Gravitational acceleration	R_f	The empirical parameter related to the flood
l_{af}	The proportion of inundation length caused by the flood on link a relative to its total length	R_{imj}	Perceived flood risk for the specific user type m on the path j which serves the O-D pair i

B. Derivation process of calculation method of 't_{ima}'

Perceived link travel times of specific user category 'm' within the same O-D pair i can be expressed as follows:

$$\Pr(T_a < t_{ima}) \geq \rho_{im}$$
$$\forall i \in I, \forall m \in M_i, \forall a \in A \tag{B.1}$$

The link travel time T_a follows a random distribution, with its mean denoted as $E[T_a]$ and variance denoted as $Var[T_a]$. In this case, applying the conventional One-side Chebyshev Inequality yields the following expression:

$$\Pr(T_a \geq E[T_a] + k) \leq \frac{var[T_a]}{var[T_a] + k^2} \tag{B.2}$$

The inequality $(B.2)$, constructed based on Chebyshev Inequality, is strictly valid. It incorporates the mathematical relationship between k, $E[T_a]$, and $var[T_a]$. Building on this relationship and applying the principles of reliability-based travel time, the connection between user risk sensitivity and perceived travel time can be further derived and expressed through an appropriate analytical solution. Set the formula $(B.2)$ as event A, then according to the definition of probability, the probability expression for the complementary event $\bar{A}$ can be obtained as follows:

$$\Pr(\bar{A}) = 1 - \Pr(A) \tag{B.3}$$

Then the Chebyshev Inequality expression for the complementary event $\bar{A}$ is:

$$\Pr(\bar{A}) = \Pr(T_a < E[T_a] + k) = 1 - \Pr(A) \geq 1 - \frac{var[T_a]}{var[T_a] + k^2} \tag{B.4}$$

Therefore, it can be deduced that:

$$\Pr(T_a < E[T_a] + k) \geq 1 - \frac{var[T_a]}{var[T_a] + k^2} \tag{B.5}$$

The purpose of constructing equation for t_{ima} is to directly correlate perceived time with the risk sensitivity of users, thus providing:

$$1 - \frac{var[T_a]}{var[T_a] + k^2} = \rho_{im} \tag{B.6}$$

Therefore, it naturally follows that:

$$\Pr(T_a < t_{ima}) \geq \rho_{im} \tag{B.7}$$

where:

$$t_{ima} = E[T_a] + \sqrt{\frac{\rho_{im}}{1 - \rho_{im}}} \cdot \sqrt{var[T_a]} \tag{B.8}$$

C. Proof of the Sub-additivity of Perceived Link Travel Time

For ease of comprehension and elucidation, here assume the path is denoted by 'j' encompassing only two links, namely 'a' and 'b', as $j = a + b$. Then according to the definition of perceived travel time in this study, perceived travel time of link a, b and path j can be expressed as:

$$t_{ima} = E[T_a] + \lambda \cdot \sqrt{var[T_a]} \tag{C.1}$$

$$t_{imb} = E[T_b] + \lambda \cdot \sqrt{var[T_b]} \tag{C.2}$$

$$\hat{t}_{imj} = E\left[T_{ij}\right] + \lambda \cdot \sqrt{var\left[T_{ij}\right]} \qquad (C.3)$$

where $\lambda = \sqrt{\frac{\rho_{im}}{1-\rho_{im}}}$.

Then based on the definition of the sub-additivity property of a risk measure, equation $(C.1)$, $(C.2)$ and $(C.3)$ need hold the following relationship:

$$\hat{t}_{imj} \leq t_{imj} = t_{ima} + t_{imb} \qquad (C.4)$$

Utilizing the $\rho_{a,b}$ represents the Pearson product-moment correlation coefficient, considering the transformation trends between path travel time and link travel time, and the value of which always holds: $0 < \rho_{a,b} \leq 1$. Then the following relationship can be derived:

$$0 < \rho_{a,b} \leq 1 \Rightarrow 0 < \frac{cov[T_a, T_b]}{\sqrt{var[T_a] \cdot var[T_b]}} < 1 \Rightarrow var\left[T_{ij}\right] - \left(\sqrt{var[T_a]} + \sqrt{var[T_b]}\right)^2 \leq 0$$

$$\Rightarrow \frac{var\left[T_{ij}\right]}{\left(\sqrt{var[T_a]} + \sqrt{var[T_b]}\right)^2} \leq 1 \Rightarrow \left(\frac{\sqrt{var\left[T_{ij}\right]}}{\sqrt{var[T_a]} + \sqrt{var[T_b]}}\right)^2 \leq 1$$

$$\Rightarrow \lambda \cdot \left(\sqrt{var\left[T_{ij}\right]} - \sqrt{var[T_a]} - \sqrt{var[T_b]}\right) \leq 0$$

$$\Rightarrow E\left[t_{ij}\right] - (E[T_a] + E[T_b]) + \lambda \cdot \left(\sqrt{var\left[T_{ij}\right]} - \sqrt{var[T_a]} - \sqrt{var[T_b]}\right) \leq 0$$

$$\Rightarrow \hat{t}_{imj} \leq t_{imj} = t_{ima} + t_{imb} \qquad (C.4)$$

D. Proof of the expression of P_{imj}

When considering only two paths, j and k, the proportion of selecting path j, is denoted as P_{imj}. Similarly, according to the definition, within the acceptable path set, the probability that the cost of path j, after applying selection inertia, is less than or equal to the cost of other acceptable paths without selection inertia is denoted as Y_{imj}, that can be expressed as the following equation:

$$Y_{imj} = \Pr\left(t_{imj} + R_{imj} - \varepsilon_{imj} \leq t_{imk} + R_{imk}, \forall k \in \bar{J}_{im}\right) \qquad (D.1)$$

Using the same criteria for judgment, as outlined in the main text regarding the definitions of R_{imj} and ε_{imj}, whether R_{imj} or ε_{imj} are mutually independent among the acceptable paths set. The derivation of Y_{imj} is based on the Random Utility Maximization theory, where the discrete term in the utility equation follows the assumption of independent and identically distributed (IID) and satisfies the Independence of Irrelevant Alternatives (IIA) assumption (McFadden, 1972). Hence, when the number of acceptable paths increases beyond two, the probability of selecting path j is expressed as follows:

$$Y_{imj} = \prod_{k \in \bar{J}_{im}, k \neq j} \Pr\left(t_{imj} + R_{imj} - \varepsilon_{imj} \leq t_{imk} + R_{imk}\right) \qquad (D.2)$$

Based on the distribution characteristics of the R_{imj}, for ease of expression, replacing '$-R_{imj}$' with 'a_{imj}', the expression concerning probability of selecting path j is as follows:

$$Y_{imj} = \prod_{k,k\neq j} \Pr\left(a_{imk} \le t_{imk} - t_{imj} + a_{imj} + \varepsilon_{imj}\right)$$

$$= \int_0^{\bar{\varepsilon}_{imj}} \frac{1}{\bar{\varepsilon}_{imj}} \cdot \int_{-\infty}^{\infty} \prod_{k,k\neq j} e^{-e^{-\left(t_{imk}-t_{imj}+a_{imj}+\varepsilon_{imj}+r_{imk}\right)}} \cdot e^{-e^{-\left(a_{imj}+r_{imj}\right)}} \cdot e^{-\left(a_{imj}+r_{imj}\right)} da_{imj} \cdot d\varepsilon_{imj}$$

$$= \frac{1}{\bar{\varepsilon}_{imj}} \cdot \int_0^{\bar{\varepsilon}_{imj}} \int_{-\infty}^{\infty} e^{-\sum_{k,k\neq j} e^{-\left(a_{imj}-t_{imj}+\varepsilon_{imj}+t_{imk}+r_{imk}\right)}} \cdot e^{-e^{-\left(a_{imj}-t_{imj}+\varepsilon_{imj}+t_{imj}+r_{imj}\right)} \cdot e^{\varepsilon_{imj}}} \cdot e^{-\left(a_{imj}+r_{imj}\right)} da_{imj} \cdot d\varepsilon_{imj}$$

$$= \frac{1}{\bar{\varepsilon}_{imj}} \cdot \int_0^{\bar{\varepsilon}_{imj}} \int_{-\infty}^{\infty} e^{-\sum_k e^{-\left(a_{imj}-t_{imj}+\varepsilon_{imj}+t_{imk}+r_{imk}\right)}} e^{-e^{-\left(a_{imj}-t_{imj}+\varepsilon_{imj}+t_{imj}+r_{imj}\right)} \cdot \left(e^{\varepsilon_{imj}}-1\right)} e^{-\left(a_{imj}+r_{imj}\right)} da_{imj} \cdot d\varepsilon_{imj}$$

$$= \frac{1}{\bar{\varepsilon}_{imj}} \cdot \int_0^{\bar{\varepsilon}_{imj}} \int_{-\infty}^{\infty} exp\left(-e^{-a_{imj}} \cdot \sum_k e^{t_{imj}-\varepsilon_{imj}-t_{imk}-r_{imk}}\right) \cdot exp\left(e^{-a_{imj}-\varepsilon_{imj}-r_{imj}} - e^{-a_{imj}-r_{imj}}\right) \cdot e^{-a_{imj}-r_{imj}} da_{imj} \cdot d\varepsilon_{imj} \qquad (D.3)$$

Next, employing the method of substitution, given $e^{-a_{imj}} = t$, in conjunction with the results from the equation $(D.3)$, we can further derive the expression for Y_{imj}:

$$Y_{imj} = e^{-r_{imj}} \cdot \frac{1}{\bar{\varepsilon}_{imj}} \int_0^{\bar{\varepsilon}_{imj}} \int_0^{\infty} \exp\left(\left(-\sum_k e^{t_{imj}-\varepsilon_{imj}-t_{imk}-r_{imk}} - e^{-r_{imj}} + e^{-\varepsilon_{imj}-r_{imj}}\right) \cdot t\right) dt \cdot d\varepsilon_{imj}$$

$$= \frac{1}{\bar{\varepsilon}_{imj}} \cdot e^{-r_{imj}} \cdot \int_0^{\bar{\varepsilon}_{imj}} \left[\frac{\exp\left(\left(-\sum_k e^{t_{imj}-\varepsilon_{imj}-t_{imk}-r_{imk}} - e^{-r_{imj}} + e^{-\varepsilon_{imj}-r_{imj}}\right) \cdot t\right)}{-\sum_k e^{t_{imj}-\varepsilon_{imj}-t_{imk}-r_{imk}} - e^{-r_{imj}} + e^{-\varepsilon_{imj}-r_{imj}}}\right]_0^{\infty} d\varepsilon_{imj}$$

$$= \frac{1}{\bar{\varepsilon}_{imj}} \cdot \int_0^{\bar{\varepsilon}_{imj}} \frac{1}{e^{-\varepsilon_{imj}} \cdot \left(\sum_k e^{t_{imj}+r_{imj}-t_{imk}-r_{imk}} - 1\right) + 1} d\varepsilon_{imj} \qquad (D.4)$$

Then, given $e^{-\varepsilon_{imj}} = s$, in conjunction with the results from the equation $(D.4)$, the following expression for Y_{imj} can be obtained:

$$Y_{imj} = \frac{1}{\bar{\varepsilon}_{imj}} \cdot \int_{e^{-\bar{\varepsilon}_{imj}}}^{1} \frac{1}{s^2 \cdot (\sum_k e^{t_{imj}+r_{imj}-t_{imk}-r_{imk}} - 1) + s} ds$$

$$= \frac{1}{\bar{\varepsilon}_{imj}} \cdot \ln\left(1 + \frac{(e^{\bar{\varepsilon}_{imj}} - 1) \cdot e^{-(t_{imj}+r_{imj})}}{\sum_k e^{-(t_{imk}+r_{imk})}}\right) \quad (D.5)$$

E. Proof of expression of Φ_{imk}

The expressions for the unacceptability factors corresponding to path k, compared with path j chosen within the set of acceptable paths are as follows:

$$\Phi_{imk} = \Pr(t_{imk} + R_{imk} - \varepsilon_{imk} \geq t_{imj} + R_{imj}, \forall j \in \bar{J}_{im})$$

$$= \Pr(-R_{imk} \leq t_{imk} - t_{imj} - R_{imj} - \varepsilon_{imk}, \forall j \in \bar{J}_{im}) \quad (E.1)$$

Then considering the distribution characteristics of the 'R_{imk}', for ease of expression, replacing '$-R_{imk}$' with 'a_{imk}', the Φ_{imk} can be expressed as:

$$\Phi_{imk} = \Pr(a_{imk} \leq t_{imk} - t_{imj} + a_{imj} - \varepsilon_{imk})$$

$$= \int_{0}^{\bar{\varepsilon}_{imk}} \frac{1}{\bar{\varepsilon}_{imk}} \cdot \int_{-\infty}^{\infty} e^{-e^{-(t_{imk}-t_{imj}+a_{imj}-\varepsilon_{imk}+r_{imk})}} \cdot e^{-e^{-(a_{imj}+r_{imj})}} \cdot e^{-(a_{imj}+r_{imj})} da_{imj} \cdot d\varepsilon_{imk}$$

$$= \frac{1}{\bar{\varepsilon}_{imk}} \cdot \int_{0}^{\bar{\varepsilon}_{imk}} \int_{-\infty}^{\infty} \exp\left(-e^{-a_{imj}} \cdot \left(e^{-(t_{imk}-t_{imj}-\varepsilon_{imk}+r_{imk})} + e^{-r_{imj}}\right)\right) \cdot e^{-r_{imj}} \cdot e^{-a_{imj}} da_{imj} \cdot d\varepsilon_{imk} \quad (E.2)$$

Given $e^{-a_{imj}} = t$, in conjunction with the results from the equation $(E.2)$, Φ_{imk} can be derived as:

$$\Phi_{imk} = \frac{1}{\bar{\varepsilon}_{imk}} \cdot e^{-r_{imj}} \cdot \int_{0}^{\bar{\varepsilon}_{imk}} \int_{0}^{\infty} \exp\left(-t \cdot \left(e^{-(t_{imk}-t_{imj}-\varepsilon_{imk}+r_{imk})} + e^{-r_{imj}}\right)\right) dt \cdot d\varepsilon_{imk}$$

$$= \frac{1}{\bar{\varepsilon}_{imk}} \cdot e^{-r_{imj}} \cdot \int_{0}^{\bar{\varepsilon}_{imk}} \left[\frac{\exp\left(-t \cdot \left(e^{-(t_{imk}-t_{imj}-\varepsilon_{imk}+r_{imk})} + e^{-r_{imj}}\right)\right)}{-e^{-(t_{imk}-t_{imj}-\varepsilon_{imk}+r_{imk})} - e^{-r_{imj}}}\right]_{0}^{\infty} d\varepsilon_{imk}$$

$$= \frac{1}{\bar{\varepsilon}_{imk}} \cdot \int_{0}^{\bar{\varepsilon}_{imk}} \frac{e^{-r_{imj}}}{e^{\varepsilon_{imk}} \cdot e^{t_{imj}-t_{imk}-r_{imk}} + e^{-r_{imj}}} d\varepsilon_{imk} \quad (E.3)$$

Then, given $e^{\varepsilon_{imj}} = s$, in conjunction with the results from the equation $(E.3)$, the following expression for Φ_{imk} can be obtained:

$$\Phi_{imk} = \frac{1}{\bar{\varepsilon}_{imk}} \cdot \int_{1}^{e^{\bar{\varepsilon}_{imk}}} \frac{1}{(s \cdot e^{t_{imj}+r_{imj}-t_{imk}-r_{imk}} + 1) \cdot s} ds$$

$$= \frac{1}{\bar{\varepsilon}_{imk}} \cdot \frac{e^{\bar{\varepsilon}_{imk}} \cdot (e^{t_{imj}+r_{imj}-t_{imk}-r_{imk}} + 1)}{e^{\bar{\varepsilon}_{imk}} \cdot e^{t_{imj}+r_{imj}-t_{imk}-r_{imk}} + 1} \quad (E.4)$$

References

ABDEL-ATY, M., KITAMURA, R. & JOVANIS, P. P. 1995. Exploring route choice behavior using geographic information system-based alternative routes and hypothetical travel time information input. *Transportation Research Record*.

ACOSTA-COLL, M., BALLESTER-MERELO, F., MARTINEZ-PEIRó, M. & DE LA HOZ-FRANCO, E. 2018. Real-Time Early Warning System Design for Pluvial Flash Floods—A Review. *Sensors,* 18**,** 2255.

AGONAFIR, C., LAKHANKAR, T., KHANBILVARDI, R., KRAKAUER, N., RADELL, D. & DEVINENI, N. 2023. A review of recent advances in urban flood research. *Water Security,* 19**,** 100141.

AI, X., HAN, Z. & ZHANG, Q. 2024. Extreme weather experience and climate change risk perceptions: the roles of partisanship and climate change cause attribution. *International Journal of Disaster Risk Reduction***,** 104511.

CARRION, C. & LEVINSON, D. 2012. Value of travel time reliability: A review of current evidence. *Transportation Research Part A: Policy and Practice,* 46**,** 720-741.

CARRION, C. & LEVINSON, D. 2013. Valuation of travel time reliability from a GPS-based experimental design. *Transportation Research Part C: Emerging Technologies,* 35**,** 305-323.

CHEN, A. & ZHOU, Z. 2010. The α-reliable mean-excess traffic equilibrium model with stochastic travel times. *Transportation Research Part B: Methodological,* 44**,** 493-513.

CHEN, Z. & ROSE, A. 2018. Economic resilience to transportation failure: a computable general equilibrium analysis. *Transportation,* 45**,** 1009-1027.

DE PALMA, A. & PICARD, N. 2005. Route choice decision under travel time uncertainty. *Transportation Research Part A: Policy and Practice,* 39**,** 295-324.

DI, X., LIU, H. X., PANG, J.-S. & BAN, X. 2013. Boundedly rational user equilibria (BRUE): Mathematical formulation and solution sets. *Transportation Research Part B: Methodological,* 57**,** 300-313.

FANG, X., LU, L., LI, Y. & HONG, Y. 2023. A Driver-Pressure-State-Impact-Response study for urban transport resilience under extreme rainfall-flood conditions. *Transportation Research Part D: Transport and Environment,* 121**,** 103819.

FOSGERAU, M. & SMALL, K. 2013. Hypercongestion in downtown metropolis. *Journal of Urban Economics,* 76**,** 122-134.

GRADECI, K., LABONNOTE, N., SIVERTSEN, E. & TIME, B. 2019. The use of insurance data in the analysis of Surface Water Flood events – A systematic review. *Journal of Hydrology,* 568**,** 194-206.

HE, H., LI, R., PEI, J., BILODEAU, J.-P. & HUANG, G. 2023. Current overview of impact analysis and risk assessment of urban pluvial flood on road traffic. *Sustainable Cities and Society,* 99**,** 104993.

HE, Y., THIES, S., AVNER, P. & RENTSCHLER, J. 2021. Flood impacts on urban transit and accessibility—A case study of Kinshasa. *Transportation Research Part D: Transport and Environment,* 96**,** 102889.

JACKSON, W. B. & JUCKER, J. V. 1982. An Empirical Study of Travel Time Variability and Travel Choice Behavior. *Transportation Science,* 16**,** 460-475.

KOETSE, M. J. & RIETVELD, P. 2009. The impact of climate change and weather on transport: An overview of empirical findings. *Transportation Research Part D: Transport and Environment,* 14**,** 205-221.

LAM, W. H. K., SHAO, H. & SUMALEE, A. 2008. Modeling impacts of adverse weather conditions on a road network with uncertainties in demand and supply. *Transportation Research Part B: Methodological,* 42**,** 890-910.

LI, F., YAN, X.-F. & DUAN, H.-F. 2019. Sustainable Design of Urban Stormwater Drainage Systems by Implementing Detention Tank and LID Measures for Flooding Risk Control and Water Quality Management. *Water Resources Management,* 33**,** 3271-3288.

LIU, H., RECKER, W. & CHEN, A. 2004. Uncovering the contribution of travel time reliability to dynamic route choice using real-time loop data. *Transportation Research Part A: Policy and Practice,* 38**,** 435-453.

LO, H. K., LUO, X. W. & SIU, B. W. Y. 2006. Degradable transport network: Travel time budget of travelers with heterogeneous risk aversion. *Transportation Research Part B: Methodological,* 40**,** 792-806.

MA, F., AO, Y., WANG, X., HE, H., LIU, Q., YANG, D. & GOU, H. 2023. Assessing and enhancing urban road network resilience under rainstorm waterlogging disasters. *Transportation Research Part D: Transport and Environment,* 123**,** 103928.

MAHMASSANI, H. S. & LIU, Y.-H. 1999. Dynamics of commuting decision behaviour under advanced traveller information systems. *Transportation Research Part C: Emerging Technologies,* 7**,** 91-107.

MARTíNEZ-GOMARIZ, E., GóMEZ, M., RUSSO, B. & DJORDJEVIĆ, S. 2018. Stability criteria for flooded vehicles: a state-of-the-art review. *Journal of Flood Risk Management,* 11**,** S817-S826.

MCFADDEN, D. 1972. Conditional logit analysis of qualitative choice behavior.
NIKOLOVA, E. & STIER-MOSES, N. E. 2014. A mean-risk model for the traffic assignment problem with stochastic travel times. *Operations Research,* 62**,** 366-382.
PATIL, V., KHADKE, Y., JOSHI, A. & SAWANT, S. 2024. Flood Mapping and Damage Assessment using Ensemble Model Approach. *Sensing and Imaging,* 25**,** 15.
PATWARY, M. M., BARDHAN, M., HAQUE, M. A., MONIRUZZAMAN, S., GUSTAVSSON, J., KHAN, M. M. H., KOIVISTO, J., SALWA, M., MASHREKY, S. R., RAHMAN, A. K. M. F., TASNIM, A., ISLAM, M. R., ALAM, M. A., HASAN, M., HARUN, M. A. Y. A., NYBERG, L. & ISLAM, M. A. 2024. Impact of extreme weather events on mental health in South and Southeast Asia: A two decades of systematic review of observational studies. *Environmental Research,* 250**,** 118436.
REN, Z., ZHAO, H., MU, X., XU, Q., SHI, K. & YANG, G. 2024. Spatiotemporal variations of extreme weather events and climate drivers in the Three Gorges Reservoir Area and its surrounding regions from 1960 to 2020. *Atmospheric Research,* 304**,** 107379.
SIMON, H. A. 1955. A Behavioral Model of Rational Choice. *The Quarterly Journal of Economics,* 69**,** 99-118.
SIRI, E., SIRI, S. & SACONE, S. 2022. A topology-based bounded rationality day-to-day traffic assignment model. *Communications in Transportation Research,* 2**,** 100076.
SIU, B. W. Y. & LO, H. K. 2014. Punctuality-based route and departure time choice. *Transportmetrica A: Transport Science,* 10**,** 585-621.
SULLIVAN, J. L., SENTOFF, K., SEGALE, J., MARSHALL, N. L., FITZGERALD, E. & SCHIFF, R. 2023. A new risk-based measure of link criticality for flood risk planning. *Transportation*.
SUMALEE, A., UCHIDA, K. & LAM, W. H. K. 2011. Stochastic multi-modal transport network under demand uncertainties and adverse weather condition. *Transportation Research Part C: Emerging Technologies,* 19**,** 338-350.
VAN OOTEGEM, L., VERHOFSTADT, E., VAN HERCK, K. & CRETEN, T. 2015. Multivariate pluvial flood damage models. *Environmental Impact Assessment Review,* 54**,** 91-100.
WANG, N., HOU, J., DU, Y., JING, H., WANG, T., XIA, J., GONG, J. & HUANG, M. 2021. A dynamic, convenient and accurate method for assessing the flood risk of people and vehicle. *Science of The Total Environment,* 797**,** 149036.
WANG, X.-J., ZHANG, J.-Y., SHAHID, S., GUAN, E.-H., WU, Y.-X., GAO, J. & HE, R.-M. 2016. Adaptation to climate change impacts on water demand. *Mitigation and Adaptation Strategies for Global Change,* 21**,** 81-99.
WATLING, D. 2006. User equilibrium traffic network assignment with stochastic travel times and late arrival penalty. *European Journal of Operational Research,* 175**,** 1539-1556.
XU, X., CHEN, A., CHENG, L. & LO, H. K. 2014. Modeling distribution tail in network performance assessment: A mean-excess total travel time risk measure and analytical estimation method. *Transportation Research Part B: Methodological,* 66**,** 32-49.
XU, X., CHEN, A., CHENG, L. & YANG, C. 2017. A link-based mean-excess traffic equilibrium model under uncertainty. *Transportation Research Part B: Methodological,* 95**,** 53-75.
YE, Q. & KIM, H. 2019. Assessing network vulnerability of heavy rail systems with the impact of partial node failures. *Transportation,* 46**,** 1591-1614.
ZHOU, R., ZHENG, H., LIU, Y., XIE, G. & WAN, W. 2022. Flood impacts on urban road connectivity in southern China. *Scientific Reports,* 12**,** 16866.